UNIVERSITY OF CALIFORNIA, SAN DIEGO

Microfluidic Advancements in Quantitative Microbiology

A dissertation submitted in partial satisfaction of the requirements for the degree of Doctor of Philosophy

in

Biology

by

Megan E. Dueck

Committee In Charge:

Professor Jeff Hasty, Chair
Professor Lin Chao
Professor Susan Golden
Professor John Guatelli
Professor Joe Pogliano

2016

The dissertation of Megan E. Dueck is approved, and it is acceptable in quality and form for publication on microfilm and electronically:

Chair

University of California, San Diego

2016

Dedication

Any successes I have had in science I owe to my mentors and the opportunities they have provided. I am forever in debt.

To my knowledge there is no history of career academics in my family lineage. I don't know where she got it from, but my older sister (by 2.5 years) has always been an academic super star (currently 134 PubMed hits!). Had she not set such a high standard, or forced me to do a good job on my homework as a young kid (while – despite my best efforts – refusing to just do it for me)… I have no idea where I would be.

My parents – who threw caution to the wind and **allegedly** illegally immigrated to the US from exotic Canada in 1978 with one toddler and one infant in tow – are also pretty badass. Thanks for everything Jack and Jacquie!

.

Epigraph

Day after day
They send my friends away
To mansions cold and grey
To the far side of town
Where the thin men stalk the streets
While the sane stay underground

Day after day
They tell me I can go
They tell me I can blow
To the far side of town
Where it's pointless to be high
'Cause it's such a long way down

So I tell them that
I can fly, I will scream, I will break my arm
I will do me harm

Here I stand, foot in hand, talking to my wall
I'm not quite right at all... am I

Don't set me free, I'm as heavy as can be
Just my librium and me
And my E.S.T. makes three

'Cause I'd rather stay here
With all the madmen
Than perish with the sad men roaming free

And I'd rather play here
With all the madmen
For I'm quite content they're all as sane as me

Day after day
They take some brain away
Then turn my face around
To the far side of town
And tell me that it's real
Then ask me how I feel

-David Bowie

Table of Contents

List of Abbreviations

3D – 3-dimensional

AHL – N-Acyl homoserine lactone

Amp – ampicillin

B. subtilis – *Bacillus subtilis*

CAMHB – cation-adjusted Mueller-Hinton broth

CAT – chloramphenicol acetyltransferase

CCD – charge coupled device

Cm – chloramphenicol

CPEC – circular polymerase extension cloning

DAW – Dial-a-Wave

DNA – deoxyribonucleic acid

E. coli – *Escherichia coli*

E. faecalis – *Enterococcus faecalis*

E. pacifica – *Euphausia pacifica*

et al. – *et alia* (which means “and others”)

Fig – figure

FRP – free running period

GFP – green fluorescent protein

h – hour

Hg – mercury

i.e. – *id est* (roughly translates to “that is”)

IPTG – Isopropyl β-D-1-thiogalactopyranoside

Kan – kanamycin

kPa – kilopascal

LB – lysogeny broth

mg – milligram

MIC – minimum inhibitory concentration

min – minute

mL – milliliter

mM – millimolar

mm – millimeter

mTorr – millitorr

nM – nanomolar

nm – nanometer

OD600 – optical density at 600 nm wavelength light

P. mirabilis – *Proteus mirabilis*

PCR – polymerase chain reaction

PDMS – polydimethyl-siloxane

$P_{lac/ara-1}$ – hybrid lac/ara-1 promoter

P_{luxI} – luxI promoter

RCF – relative centrifugal force

RNA – ribonucleic acid

s – second

S. rosetta – *Salpingoeca rosetta*

scfm O_2 – Standard cubic feet per minute oxygen

sec – second

Spect – spectinomycin

Tet – tetracycline

Vanc – vancomycin

w/v – weight per volume

µg – microgram

µL – microliter

µm – micrometer

µM – micromolar

List of Figures

List of Tables

Acknowledgements

Chapter 3 contains material originally published as: Halperin SO, Poling CT, Mathrani SR, Turner BW, Greene AC, Dueck ME, Myers F (2014) A massively parallel microfluidic device for long-term visualization of isolated motile cells. Microfluidics and nanofluidics 17(5): 821-829.

Chapter 4 contains material originally published as: Cira NJ, Ho JY, Dueck ME, Weibel DB (2012) A self-loading microfluidic device for determining the minimum inhibitory concentration of antibiotics. Lab on a Chip 12(6): 1052-1059.

This work was supported, in part by the National Institutes of Health Cell and Molecular Genetics training grant.

Vita

Arizona State University

2002 Bachelor of Science, Biology

University of California, San Diego

2005 Master of Science, Molecular Pathology

University of California, San Diego

2016 Doctor of Philosophy, Biology

PUBLICATIONS

Peer Reviewed Journal Articles

Halperin SO, Poling CT, Mathrani SR, Turner BW, Greene AC, Dueck ME, Myers FB (2014) A massively parallel microfluidic device for long-term visualization of isolated motile cells. Microfluidics and nanofluidics 17(5): 821-829.

Sochol RD, Dueck ME, Li S, Lee LP, Lin L (2012) Hydrodynamic resettability for a microfluidic particulate-based arraying system. Lab on a Chip 12: 5051-5056.

Cira NJ, Ho JY, Dueck ME, Weibel DB (2012) A self-loading microfluidic device for determining the minimum inhibitory concentration of antibiotics. Lab on a Chip 12(6): 1052-1059.

Sochol RD, Casavant BP, Dueck ME, Lee LP, Lin L (2011) A dynamic bead-based microarray for parallel DNA detection. Journal of Micromechanics and Microengineering 21(5): 1039-1048.

Nevill JT, Cooper R, Dueck M, Breslauer DN, Lee LP (2007) Integrated microfluidic cell culture and lysis on a chip. Lab on a Chip 7(12):1689-95. [Selected as cover page article and one of the most accessed Lab on a Chip articles of November and December.]

Dueck M, Guatelli JC (2007) Evidence against a direct antiviral activity of the proteasome during the early steps of HIV-1 replication. Virology 361(1):1-8.

Tang S, Ablan S, Dueck M, Ayala-Lopez W, Soto B, Caplan M, Nagashima K, Hewlett IK, Freed EO, Levin JG (2007) A second-site suppressor significantly improves the defective phenotype imposed by mutation of an aromatic residue in the N-terminal domain of the HIV-1 capsid protein. Virology. 359(1):105-15.

Day JR, Martinez LE, Sasik R, Hitchin D, Dueck M, Richman DD, Guatelli JC (2006) A computer-based, image-analysis method to quantify HIV-1 infection in a single-cycle infectious center assay. Journal of Virological Methods 137(1): 125-133.

Abstract Of The Dissertation

Microfluidic Advancements in Quantitative Microbiology

by

Megan E. Dueck

Doctor of Philosophy in Biology

University of California, San Diego, 2016

Professor Jeff Hasty, Chair

Microfluidic technologies have allowed modern microbiologists the opportunity to explore biological phenomenon in ground-breaking new ways. The rapid prototyping capability of standard polydimethyl-siloxane (PDMS) microfluidic devices has put the design and optimization of these innovative

new tools directly into the hands of the microbiologists who are using them. This has caused a dramatic surge in the utilization of these devices by biological researchers in the past several years. In this dissertation I present original research in which microfluidic technologies were used to advance quantitative microbiology. To provide context, in chapter 1 I highlight several key areas of research and seminal previous works where microfluidic technologies have expanded the horizon for microbial exploration. In the chapters that follow I present 3 separate bodies of original research. In chapter 2 I present a study where a novel synthetic gene oscillator is entrained to environmental oscillations through an engineered fitness advantage. In this particular study, microfluidic devices allowed for the monitoring and quantitative analysis of individual genetically engineered *E. coli*. In chapter 3 I present a microfluidic platform for quantitatively studying motility phenotypes in arrayed chambers of microorganisms. In chapter 4 I present a microfluidic platform for improved bacterial antibiotic susceptibility testing.

Chapter 1: Background

1.1 Microfluidics and Microbiology

Our understanding of the scientific world is limited by the technologies available to us for exploration. Early microbiologists were limited to macroscale glassware, rudimentary microscopes and low-resolution assays. Even as recently as several decades ago, scientists largely relied on low-throughput technologies, test tubes and agar plates. Nowadays a microbiologist can run a matrix of 3,456 experimental conditions on a single multi-well plate. While these sorts of multi-well plates do allow for massively multiplexed experimentation, they still do not address several fundamental limitations of classic microbiology. Historically if a researcher wanted to change the media conditions of their growing microbes, the researcher would need to pause their experiment and then physically swap out the media either by hand or - in recent times - using a pipetting robot. If a researcher was doing live-imaging, they would need to pause the imaging and physically remove the experiment from the microscope to alter the cells' chemical environment. Similarly, it was historically impossible for researchers to expose a single population of growing microorganisms to a gradient of chemical conditions within a solitary vessel.

The advent of microfluidics and rapid microdevice prototyping has inarguably broadened the scope of questions that a modern microbiologist can answer. A researcher can now completely alter the chemical environment of

growing cells almost instantaneously, and then moments later completely switch it again, all while doing continuous microscopic imaging. Exploiting the laminar flow that occurs in microscale channels, a researcher studying chemotaxis can now expose a single growing colony of microorganisms to a stable gradient of chemicals. In a test-tube or multi-well plate, the composition of liquid media changes as microorganisms grow and divide. Microfluidic devices allow for constant perfusion of fresh media across chambers of growing cells. This allows a researcher to know the precise chemical environment of their microorganisms at all times.

In this dissertation I present 3 separate bodies of work where microfluidic technologies have been used to advance quantitative biology. As an introduction to this original research, I will highlight several areas of research and seminal publications where biological phenomenon have been examined in a way that was not possible prior to the rise of microfluidic technologies.

1.2 Precise Tracking of Individual Microbial Cells

In nature microorganisms grow in 3-dimensional space where they can form complex colony patterns and dense biofilms. When not confined, microorganisms in a dish will behave similarly in that they will grow both outward and upward. This has hindered researchers ability to precisely image individual live cells. Microfluidic devices allow researchers to confine microorganisms in the upward direction, while allowing them to freely grow and divide in the outward

direction. In doing this, a researcher can force microbial cells to grow in monolayers, allowing for the observation and tracking of individual cells.

In a groundbreaking study by Balaban *et al.* (2004) a microfluidic device was used to grow *E. coli* in microscale cell-width, cell-depth grooves (Figure 1.1). After seeding sparsely spaced individual cells in these grooves, the cells were imaged as they grew and divided. This allowed researchers to track *E. coli* lineages in a way that had previously not been possible. They used this ability to examine the relationship between gene expression dynamics and bacterial antibiotic persistence. They showed that individual lineages could spontaneously switch growth phenotypes. Ultimately they concluded that antibiotic persistence was linked to gene expression heterogeneity within a population. Their results provided evidence that gene expression heterogeneity across a population may be an adaption that allows bacteria to survive in a dynamically changing environment. While this microfluidic device was critical to this study, it was also complex to fabricate as it involved multiple layers and fabrication steps. In 2010 Wang *et al.* revisited the idea of growing *E. coli* in cell-sized grooves in a device they named “the Mother machine”. In a design that resembles a comb, this device has thousands of teeth-like channels coming off of a larger and deeper main channel. These “comb teeth” are cell-width, the length of several cells in a line, and only open to the main channel on one end (Figure 1.2). The device is loaded such that cells reach the blunt, dead-end of each “comb tooth”. Since cells can only escape from one end of the channel, this allows for precise

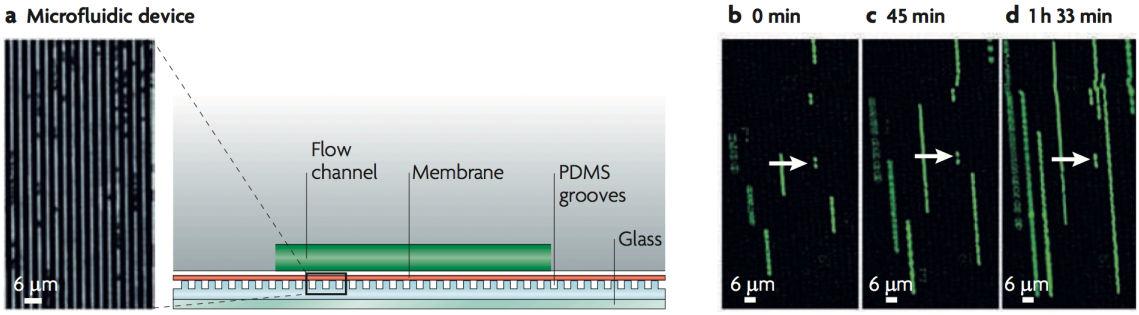

Figure 1.1: *E. coli* grown in microgrooves. a) Design of a multilayer microfluidic device for imaging and tracking of cell lineages that spawn from an individual *E. coli*. b) An image highlighting an individual *E. coli* cell after seeding and then its growth after c) 45 minutes and d) 1 hour and 33 minutes. Figure reproduced from Balaban *et al.* (2004).

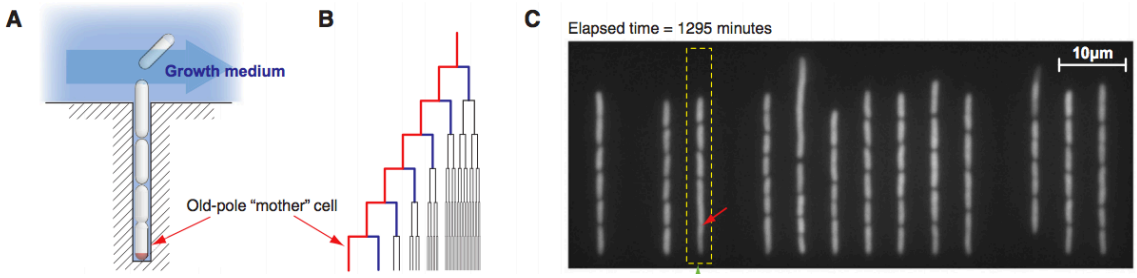

Figure 1.2: *E. coli* grown in "Mother Machine". A) Design of a microfluidic device for trapping and holding an individual *E. coli* cell as its daughter cells bud off and eventually exit the trap. B) A schematic highlighting the retention of the same cell pole during imaging. C) A microscopic image of the "Mother Machine" loaded with fluorescently labeled *E. coli*. Figure reproduced from Wang *et al.* (2010).

tracking of the initial “Mother cell”. They showed that the mother cell inherited the same pole for hundreds of generations. They also provide evidence that accumulation of damage is a measurable factor for predicting cell death.

In a similar fashion to the aforementioned “Mother Machine”, in 2006 Ryley *et al.* developed a device in which individual yeast where trapped in cell-sized “jails” (Figure 1.3). These “jails” had openings large enough to allow budding daughter cells to escape and flush away, while confining the mother cell. They used this device to track changes in gene expression in an individual cell over time. Using this device they showed temporal variation in the expression levels of both HSP104 and RAS2. These fluctuations had not been seen using any other single-cell analysis tool. As with the 2004 Balaban study, this device provided an avenue for scientific exploration that had not existed prior, but was tedious to fabricate and use. Recently Jo *et al.* (2015) developed an improved “mother-trapping, daughter-releasing” device that they used to explore aspects of yeast replicative aging (Figure 1.4).

1.3 Exploring Microbial Dynamics at the Population Level

Natural microbial biofilms can produce beautifully intricate shapes and patterns. These morphologies are the result of interactions between cells within the population. Exploring intracellular communication is key to understanding microbial ecology. Some researchers attempt to recreate observable microbial

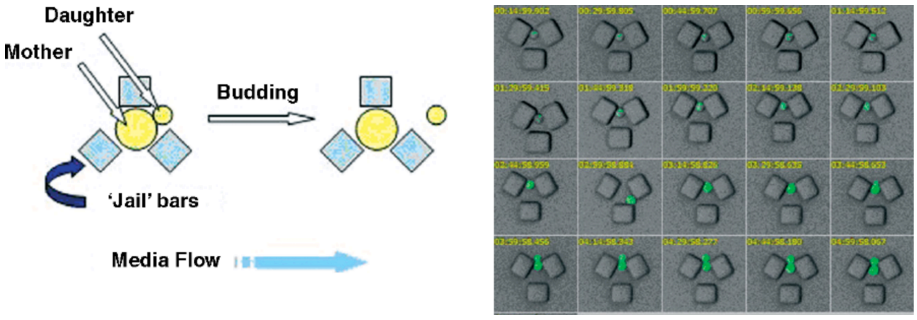

Figure 1.3: Yeast grown in microfluidic "jails". Schematic and microscopic images of yeast cells trapped in microfluidic "jails" that allow a daughter cell to bud off and exit the jail while the mother cell is retained. Figure reproduced from Ryley *et al.* (2006).

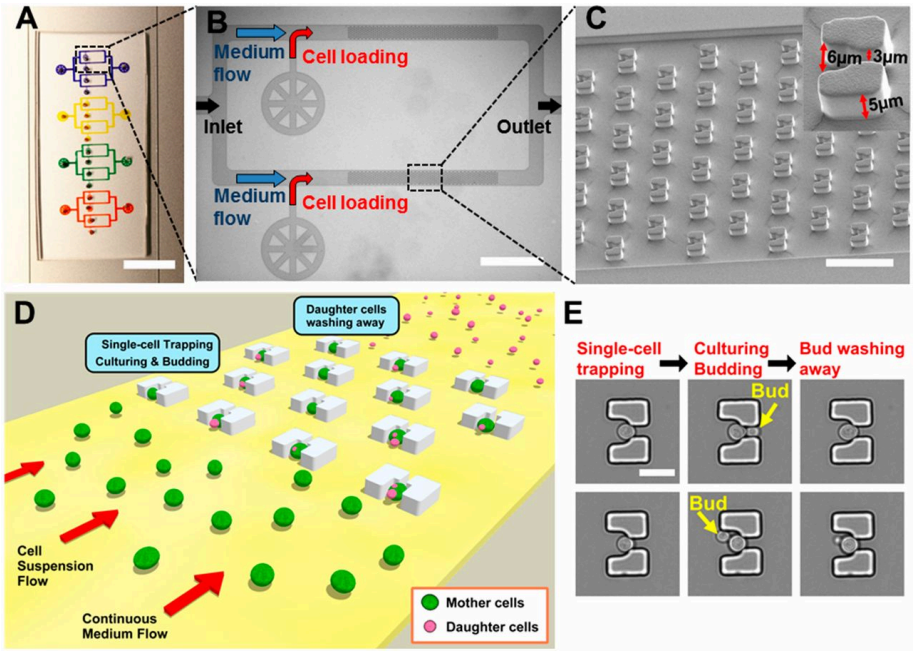

Figure 1.4: Yeast grown in arrayed single cell traps. A, B & C) Microfluidic device images and specifications. D) Schematic of yeast cell loading. E) Microscopic images showing a daughter cell bud off and wash away while the mother cell is retained. Figure reproduced from Jo *et al.* (2015).

ecology phenotypes in the lab. Microfluidics allows these researchers an additional tool to modify the inorganic architecture of an artificially created microbial community.

In nature individual microbial species do not exist in a bubble. Their existence is shaped by the other species with whom they share a community. In 2008 Kim *et al.* used a microfluidic approach to explore interactions between 3 different soil bacterial species. They developed a device in which the 3 different species were physically prohibited from growing into the same space by being confined to independent chambers. These confined chambers did, however, allow for chemical communication across a diffusive membrane barrier with nano-scale pores (Figure 1.5). In a standard well-mixed liquid culture one of the species would take over to the detriment of the other 2 species. Within their device they found that when physically separated but allowed to chemically communicate, one species would take the lead on providing a unique function that was required for the survival of the other two species. They describe the interaction they observed as being “reciprocal syntrophy”.

Bacteria in the human body often exist in distinct but linked physiological niches. In 2011 Zhang *et al.* attempted to mimic this arrangement with a microfluidic device that consisted of 1200 honeycomb-shaped microhabitats interconnected by small channels. These small connecting channels allowed for bacteria to migrate into neighboring honeycombs. The periphery of this grid of

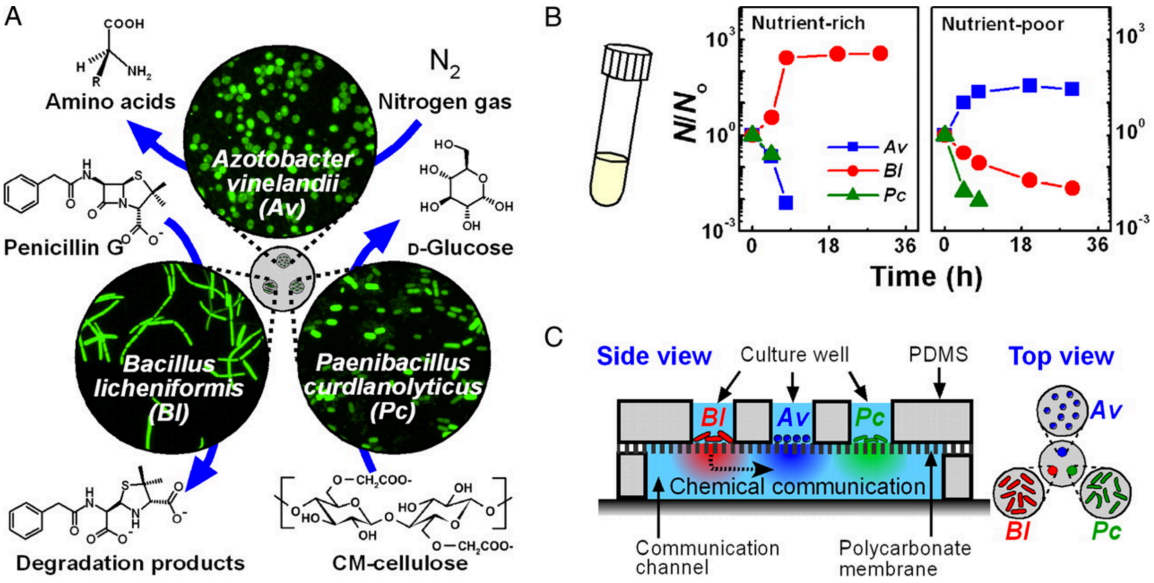

Figure 1.5: "Reciprocal syntrophy" in soil bacteria. A) Schematic depicting "reciprocal syntrophy" between 3 strains of soil bacteria. B) Graphs showing the survival ratio of each species (N/N_o) vs. time when cultured in a standard test tube liquid culture under nutrient rich and nutrient poor conditions. These show that successful co-existence between the 3 species requires physical growth barriers. C) Schematic of microfluidic device. Figure reproduced from Kim *et al.* (2008).

cell chambers was surrounded by a fluidic channel from which chemicals could diffuse into the honeycomb grid, but within which bacteria could not enter (Figure 1.6). This was used to create stable gradients of both antibiotics and nutrients across the honeycomb array. Using this device they observed that there were specific “Goldilocks points” within the micro-habitat array that were ideally suited for the emergence of antibiotic resistance. Within their microhabitat array *E. coli* developed resistance to the antibiotic ciprofloxacin within 10 hours. This was significantly more rapid than had previously been observed in any artificial bacterial growth environment.

1.4 Making Use of Controllable Fluid Dynamics

In 2008 the lab of Jeff Hasty pioneered a method for exploiting microfluidics to do live, continuous imaging of microbial cells in a dynamically changing chemical environment. In a paper by Bennett *et al.* (2008) the Hasty group introduced what they named the “Dial-a-Wave” system. This system relies upon laminar flow and gravity-driven perfusion of fluids through microscale channels. In microscale channels, where Reynold’s numbers are <1, fluids flow laminarly (without turbulence), causing fluids to primarily mix through diffusion. The key microscale feature of the Dial-a-Wave system involves 2 inlet microchannels that meet and then branch off in 2 directions: toward downstream cell chambers or toward an outlet waste port. The two inlet microchannels are connected to open-ended macroscale fluid reservoirs by tubing. If the fluid reservoirs for both inlet channels are of equal heights, the fluid flow toward the

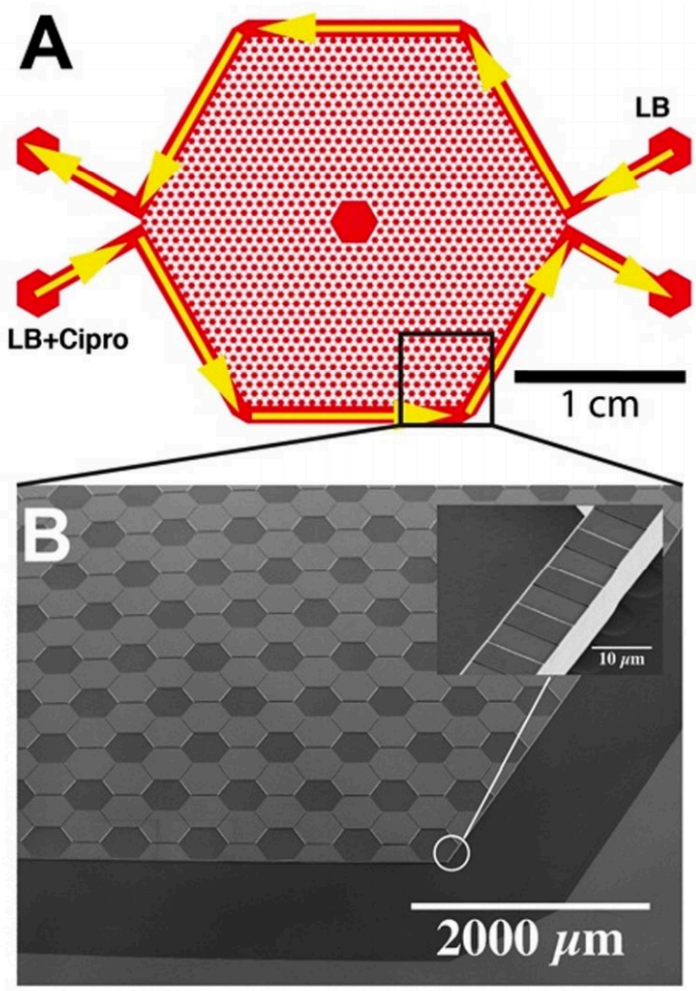

Figure 1.6: Goldilocks device. A) Schematic and B) electron micrograph of the microfluidic device used to examine rapid emergence of antibiotic resistance in *E. coli*. The device creates a gradient of both antibiotics from one side and nutrients from the other across a central array of interconnected growth niches. Figure reproduced from Zhang *et al.* (2011).

cell chambers will be 50% fluid from reservoir 1 and 50% fluid from reservoir 2. As the flow is laminar, these 2 fluids will flow side-by-side until eventually they mix through diffusion. If the fluid height in reservoir 1 is raised higher than reservoir 2, the cell-feeding channel will be comprised entirely of fluid from reservoir 1. If tuned correctly, there will still be fluid from reservoir 2 flowing through the device, toward the outlet port. When tuned in such a way, fluids from both reservoir 1 and reservoir 2 are constantly flowing through the microfluidic device, regardless of which fluid is being diverted toward the cell chambers. This allows for very rapid and programmable cell media changes. Fine-tuning also allows a researcher to feed cells specific ratios of fluids from reservoir 1 and reservoir 2 (Figure 1.7).

In 2014 Rusconi *et al.* exploited the ability to precisely control fluid dynamics in a microfluidic device to explore the effects of shear stress on bacteria. They tracked the movements and location of motile *B. subtilis* cells in a serpentine microfluidic channel with finely controlled and computationally modeled laminar flow. In doing this they were able to show that fluid shear stress effected the overall spatial distribution of the cells. The cells became “trapped” in areas of high-shear stress. This resulted in the majority of the cells being depleted from low shear regions of the microfluidic channel. This result, they ultimately concluded, can result in increased surface attachment and hindrance of chemotaxis.

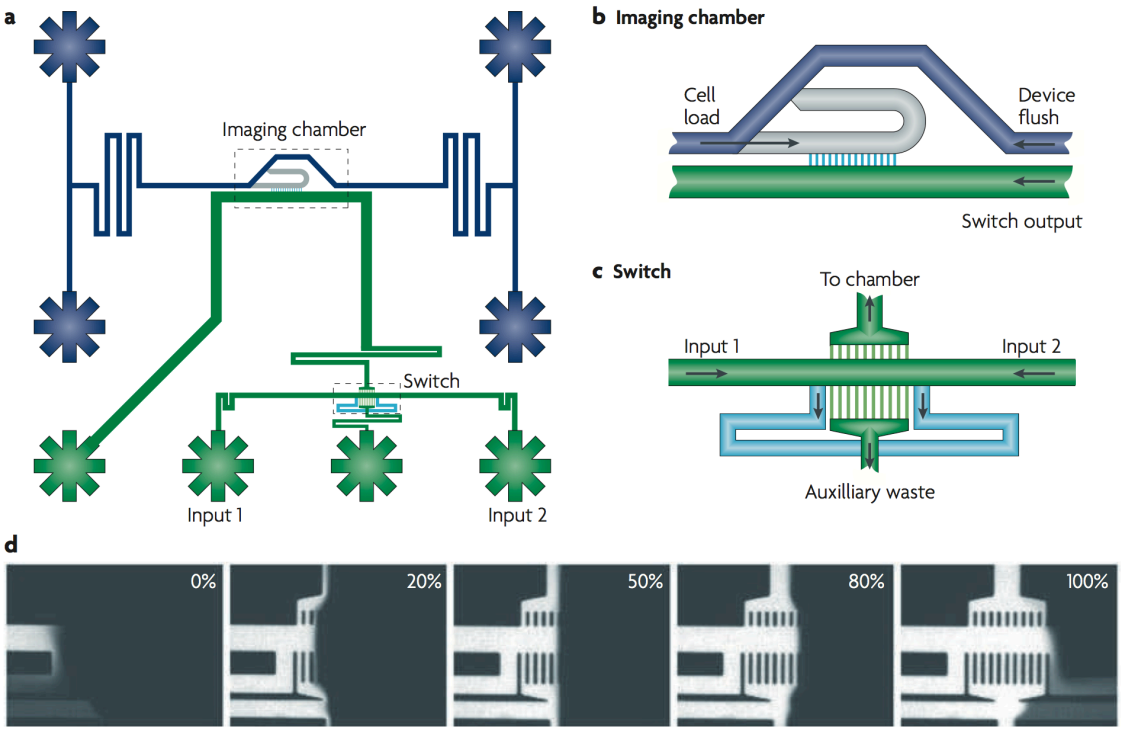

Figure 1.7: "Dial-a-Wave" dynamic microfluidic culture. a) Design of a microfluidic device containing: b) a chamber for imaging monolayers of growing yeast cells and c) a feature named the "Dial-a-Wave" that allows for rapid and tunable media changes perfused across the cell monolayer. d) Fluorescent microscope images showing the "Dial-a-Wave" generating precise ratios of 2 separate media inputs. Figure reproduced from Bennett *et al.* (2009).

1.5 Microdroplets and Microbiology

While still somewhat in its scientific infancy, microfluidics has become the predominating technology for certain tasks. The rapid production of regularly sized microdroplet emulsions is one such task. Microfluidic droplets have been used for an expansive array of applications. Even under the umbrella of microbiology, their uses have been vast. Encapsulating microorganisms in microdroplets essentially provides researchers with a method to work with and manipulate a nearly infinite number of micro-bioreactors. For example, in 2011 Park *et al.* showed that microdroplets could be used to study microbial interactions. They demonstrated this by creating droplets containing 2 strains of bacteria, each lacking the ability to synthesize a different essential amino acid. This micro-co-culture allowed both strains to grow symbiotically within an individual microdroplet.

Microdroplets also may find utility in microbial diagnostics. In 2014 Kang *et al.* demonstrated that they could detect bacteria within blood samples using a DNAzyme-based sensor (Figure 1.8). The blood sample and sensor were co-encapsulated into droplets. If the blood sample contained a specific bacterial species, a specific molecule released by that bacterial cell would result in a conformation change to the DNAzyme sensor. This change would lead to cleavage of a fluorescence quencher and a detectable fluorescent signal. Multiple groups have examined the possibility of using microdroplets as a means to improve antibiotic susceptibility testing. Baraban *et al.* (2011) used “millifluidic

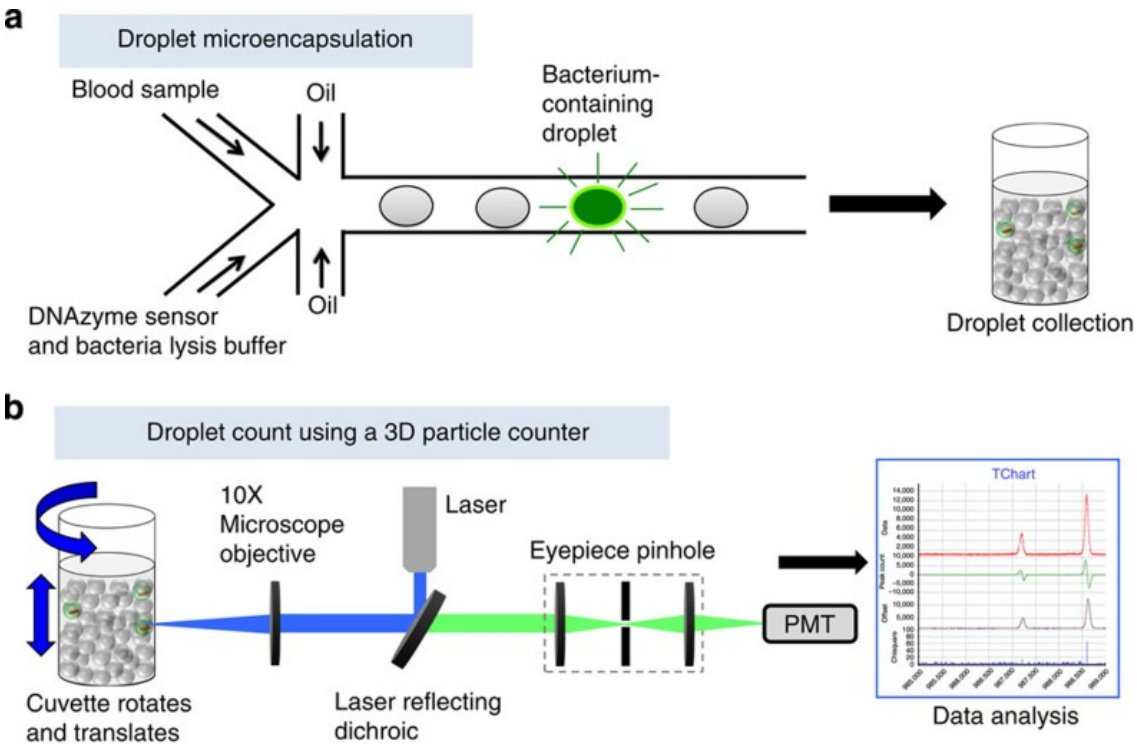

Figure 1.8: DNAzyme bacterial detection. a) Schematic showing a microfluidic feature generating microdroplets containing a blood sample, a DNAzyme sensor and bacterial lysis buffer. b) Schematic showing the analysis of microdroplets by a 3D particle counter. Figure reproduced from Kang *et al.* (2014).

droplets" to examine the effects of a matrix of antibiotic pairs on bacterial growth. Similarly Churski *et al.* (2012) exploited traditional microdroplets to examine growth phenotypes under antibiotic combinations. The impressively complete microfluidic platform that they presented would allow users to specify precise antibiotic conditions for a sequence of droplets. The sequence and chemical make-up of the droplets was recorded. This sequence of droplets was then incubated in a stretch of tubing while maintaining the precise order of the chain of droplets. After allowing time for growth, the tubing was then plugged into a device designed to measure cell growth within each successive droplet.

Microbial biotechnology applications of microdroplets have also been proposed. Huang *et al.* (2015) exploited microfluidics to screen a yeast mutant library (Figure 1.9). After bulk UV irradiation, mutant yeast were encapsulated into droplets such that each contained 1 or zero individual cells. These droplets were fabricated to contain a fluorescent substrate for the enzyme α-amylase. Increased fluorescence within a droplet indicated that the yeast within the droplet were more efficiently producing the commercially important α-amylase protein product. These desirable mutants could than be isolated and cloned. Similarly, Kim *et al.* (2016) designed an assay where droplets were used to screen microalgae for optimal growth and oil production. They demonstrated a stream-lined work-flow involving digitization of microalgae within droplets, incubation of microalgae-containing droplets, addition of fluorescent indicator dyes for growth and oil production to the droplets, and finally droplet fluorescence analysis.

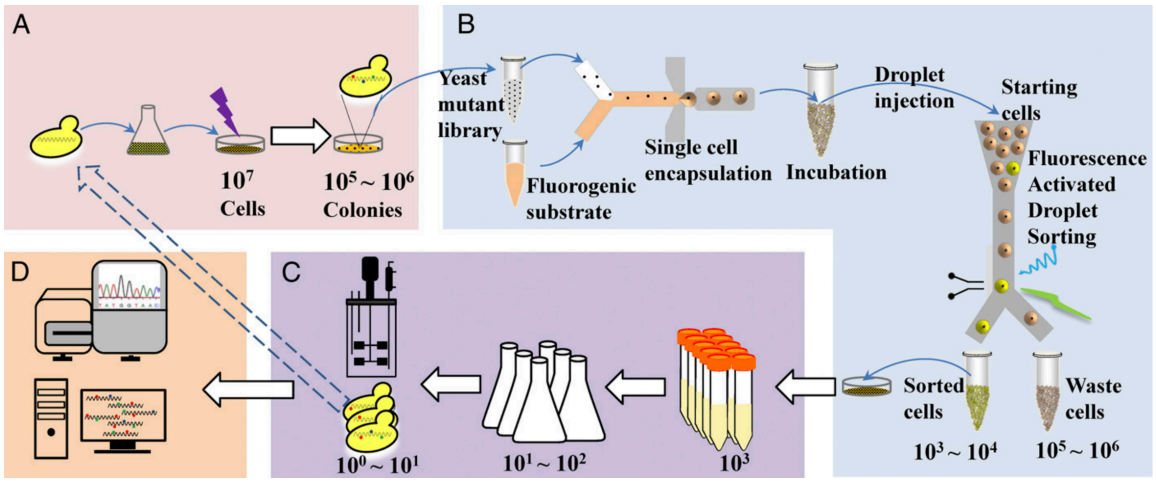

Figure 1.9: High-throughput yeast mutant phenotyping. Schematic of a work-flow for use of microdroplets to screen a yeast mutant library for increased α-amylase production. A) Initial UV irradiation to create library of mutants, B) digitization of individual mutant cells within microdroplets, incubation of microdroplets and FACS of droplets to sort out desirable clones, C) clone amplification and finally D) sequencing of desirable clones. Figure reproduced from Huang *et al.* (2015).

1.6 In Closing

This brief review of areas of microbiology that have benefited from microfluidic technology is far from comprehensive. I merely sought to highlight some key examples where microfluidics has provided an avenue for scientific exploration or measurement that was not available to microbiologists in the past. In the chapters to follow I present 3 separate bodies of original research. In Chapter 2 I present a study in which microfluidic devices allowed for precise tracking of individual genetically engineered *E. coli*. In the work described in Chapter 3 microfluidic technology was used to isolate and track the movement of motile microorganisms. In Chapter 4 a microfluidic device for improved antibiotic susceptibility testing is characterized. In each of these studies, microfluidic technology was used to advance a particular aspect of quantitative microbiology.

1.7 References

Balaban NQ, Merrin J, Chait R, Kowalik L, Leibler S (2004) Bacterial persistence as a phenotypic switch. Science 305, 1622–1625.

Baraban L, Bertholle F, Salverda ML, Bremond N, Panizza P, Baudry J, de Visser JA, Bibette J (2011) Millifluidic droplet analyser for microbiology. Lab Chip 11(23):4057-62.

Bennett MR, Pang WL, Ostroff NA, Baumgartner BL, Nayak S, Tsimring LS, Hasty J (2008) Metabolic gene regulation in a dynamically changing environment. Nature 454(7208):1119-22.

Bennett MR1, Hasty J (2009) Microfluidic devices for measuring gene network dynamics in single cells. Nat Rev Genet. 10(9):628-38.

Churski K, Kaminski TS, Jakiela S, Kamysz W, Baranska-Rybak W, Weibel DB, Garstecki P (2012) Rapid screening of antibiotic toxicity in an automated microdroplet system. Lab Chip. 12:1629–1637.

Huang M, Bai Y, Sjostrom SL, Hallström BM, Liu Z, Petranovic D, Uhlén M, Joensson HN, Andersson-Svahn H, Nielsen J (2015) Microfluidic screening and whole-genome sequencing identifies mutations associated with improved protein secretion by yeast. Proc Natl Acad Sci U S A. 112(34):E4689-96.

Jo MC, Liu W, Gu L, Dang W, Qin L (2015) High-throughput analysis of yeast replicative aging using a microfluidic system. Proc Natl Acad Sci U S A. 112(30):9364-9.

Kang DK, Ali MM, Zhang K, Huang SS, Peterson E, Digman MA, Gratton E, Zhao W (2014) Rapid detection of single bacteria in unprocessed blood using Integrated Comprehensive Droplet Digital Detection. Nat Commun. 5:5427.

Kim HJ, Boedicker JQ, Choi JW, Ismagilov RF (2008) Defined spatial structure stabilizes a synthetic multispecies bacterial community. Proc Natl Acad Sci USA. 105:18188–18193.

Kim HS, Guzman AR, Thapa HR, Devarenne TP, Han A (2016) A droplet microfluidics platform for rapid microalgal growth and oil production analysis. Biotechnol Bioeng 113(8):1691-701.

Park J, Kerner A, Burns MA, Lin XN (2011) Microdroplet-enabled highly parallel co-cultivation of microbial communities. PLoS One 6(2):e17019.

Rusconi R, Guasto JS, Stocker R (2014) Bacterial transport suppressed by fluid shear. Nature Physics 10, 212–217

Ryley J, Pereira-Smith OM (2006) Microfluidics device for single cell gene expression analysis in *Saccharomyces cerevisiae*. Yeast 23, 1065–1073.

Wang P, Robert L, Pelletier J, Dang WL, Taddei F, Wright A, Jun S (2010) Robust growth of *Escherichia coli*. Curr Biol. 20(12):1099-103.

Zhang Q, Lambert G, Liao D, Kim H, Robin K, Tung CK, Pourmand N, Austin RH (2011) Acceleration of emergence of bacterial antibiotic resistance in connected microenvironments. Science 333:1764–67

Chapter 2: Phenotypic Entrainment of a Synthetic Gene Oscillator

2.1 Abstract

Natural clock-like gene networks often operate at a defined phase shift with respect to an external process, which is maintained via entrainment by environmental cues. Entrainment critically depends on a phase-dependent sensitivity of the oscillator to the external signal. We explicitly engineered this sensitivity into a synthetic gene oscillator in *E. coli* via the periodic expression of the antibiotic resistance gene chloramphenicol acetyltransferase (CAT). We show that this new oscillator entrains to periodic environmental chloramphenicol signals and does so more efficiently than an oscillator with non-oscillatory CAT expression tuned to have the same average sensitivity to chloramphenicol. The degree of entrainment differs significantly across periods and amplitudes of the chloramphenicol pulses and our quantitative analysis reveals a classical Arnold tongue for one-to-one entrainment. We also analyze the phase difference between the oscillator and the signal, whose dependence on signal period is consistent with the hypothesis that periodic CAT expression presents windows of opportunity for the environment to interact with the host cell. We therefore propose this circuit as a model system to study “phenotypic entrainment”, where the effect of the stimulus on oscillator dynamics is caused by direct interaction of the environment with the host cell, but the cell oscillates between more and less sensitive phenotypes.

2.2 Introduction

Synthetic gene oscillators provide a bottom-up approach to understanding naturally occurring, wave-like patterns of gene expression. In addition to elucidating fundamental biological phenomena, research involving engineered gene oscillators may also improve industrial processes (Sowa 2014) or serve as novel components for future bio-sensors (Prindle 2012). The earliest synthetic gene oscillator to be tested *in vivo* - the "Repressilator" - relied upon a domino-like loop of repressor modules wherein each gene product repressed a downstream expression cassette (Elowitz 2000). Most subsequent synthetic oscillators have relied upon coupled positive and negative transcription feedback loops (Atkinson 2003, Stricker 2008, Danino 2010, Hussain 2013, Ryback 2013). One notable exception was the Fung *et al.* "matabolator", in which gene oscillations were driven by metabolic flux (Fung 2005). Cell-free synthetic gene oscillators have also been developed (Kim 2011) and later exploited to drive the periodic opening and closing of DNA nanotweezers (Franco 2011).

In nature the interaction between biological clocks and the environment can shift the phase and period of gene oscillations in a process known as entrainment. The first generation of synthetic gene oscillators achieved similar oscillatory periods across populations of cells, but phases between cells were not linked. Since then several strategies have been used to synchronize oscillatory phases across a population of cells. Using an existing non-synchronous synthetic gene oscillator, Mondragón-Palomino *et al.* entrained a population of

cells by oscillating the presence of an activator molecule that directly interacted with the synthetic clock promoter elements (2011). Danino *et al.* added quorum-sensing and quorum-quenching components to the basic positive/negative transcription feedback loop oscillator architecture to create an oscillatory strain that auto-synchronized across a population in an otherwise chemostatic environment (2010). Prindle *et al.* were able to couple discrete synthetic clocks using native bacterial queueing machinery and competitive protein degradation (2014). Chen *et al.* achieved synchronized gene oscillations in 2 genetically distinct bacterial strains by engineering each strain to produce molecules that regulate transcription in the opposing strain (2015). While not on a population-level, recently Dies *et al.* attempted to couple oscillator frequency with the cell cycle by having the oscillator drive components of the cell's chromosomal replication machinery (2016).

In this study we describe a method of population synchronization in which an oscillated synthetic gene product entrains to an oscillating environmental factor through an engineered fitness advantage. A strain of *E. coli* was engineered to have the expression of chloramphenicol acetyltransferase (CAT) - the enzyme that confers resistance to the drug chloramphenicol - driven by a traditional positive/negative transcription feedback loop oscillator. The oscillator we present is identical in architecture to that originally described by Stricker *et al.* in 2008 with an additional cassette for oscillated expression of ssrA-tagged CAT. A nearly identical control strain was also created that contains the Stricker

oscillator with an additional cassette for N-Acyl homoserine lactone (AHL)-tunable expression of non-oscillatory ssrA-tagged CAT. Both the "CAT Oscillator" and "Control Oscillator" oscillate the expression of ssrA-tagged GFP.

First we determined a level of AHL at which the Control Oscillator has matched chloramphenicol sensitivity to the CAT Oscillator. The drug chloramphenicol acts by inhibiting amino acid chain elongation by the ribosome. As such, when put into an environment at toxic levels of oscillating chloramphenicol, both the Control Oscillator and the CAT Oscillator entrained their GFP expression to the period and phase of the oscillating chloramphenicol. At toxic levels of chloramphenicol, it is likely that all gene expression would "entrain" as cellular translation is simply being turned on and off. However, when in media conditions that confer equal chloramphenicol sensitivity, the CAT Oscillator strain will entrain its GFP expression at significantly lower drive amplitudes than the Control Oscillator strain. Since both CAT and GFP are behind the same hybrid promoter in the CAT Oscillator strain, if GFP expression is entrained, it is likely that CAT expression is also entrained.

Despite biology's natural ability to entrain to its given environment, it is believed there is a fitness advantage associated with having biological rhythms that are most closely resonant with environmental rhythms (Ouyang, 1998). Relatedly, here we show that entrainment of our CAT Oscillator is strongest at chloramphenicol periods close to the average free-running period of the CAT

Oscillator, with the strongest entrainment occurring at chloramphenicol periods slightly longer than the average free-running period. Additionally, entrainment at chloramphenicol periods longer than the CAT Oscillator free-running period resulted in a period-dependent phase shift in the alignment of peak GFP expression with the environmental chloramphenicol drive. Since this method of synchronization involves a gene product's interaction with its environment, we describe the data we are presenting as an example of "phenotypic entrainment".

2.3 Results and Discussion

Genetic Circuitry

Two synthetic gene oscillators were constructed and transformed into the JS006 strain of *E. coli:* the “CAT Oscillator” and the “Control Oscillator” (Figure 2.1). Both are driven by the synthetic oscillator originally constructed by Stricker *et al.* in 2008. The Stricker (2008) oscillator is comprised of activator and repressor components driven by the hybrid lac/ara promoter (Lutz 1997). This hybrid lac/ara-1 promoter is activated by AraC in the presence of arabinose and repressed by LacI in the absence of Isopropyl β-D-1-thiogalactopyranoside (IPTG). The original Stricker (2008) oscillator contained 3 proteins behind independent copies of this hybrid lac/ara promoter: araC, lacI and GFP. The araC and lacI genes were responsible for driving the gene oscillations whereas GFP merely acted as a reporter for oscillated promoter activity. All 3 of these proteins were tagged with carboxy-terminal ssrA rapid degradation tags. The

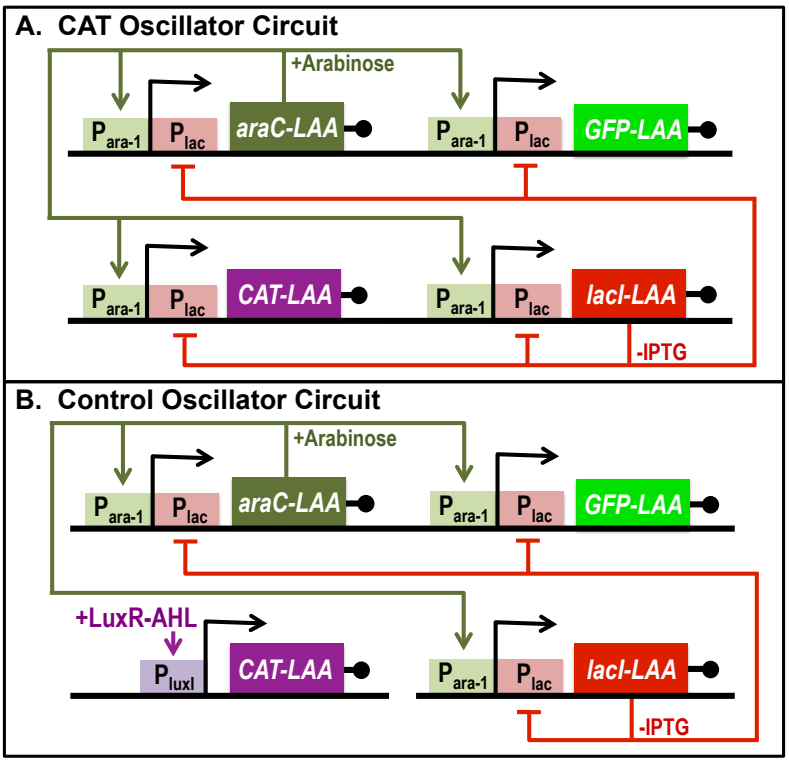

Figure 2.1: Synthetic oscillator circuitry. Both the CAT and Control Oscillator are based on the synthetic oscillator by Stricker *et al.* (2008) with additional genetic components. A) The CAT Oscillator contains an additional cassette comprised of ssrA-tagged CAT behind an additional copy of the hybrid ara-1/lac promoter. GFP acts as a reporter for both oscillatory behavior and CAT expression. B) The Control Oscillator contains an additional cassette comprised of ssrA-tagged CAT behind the luxI promoter. CAT expression is non-oscillatory and tunable with exogenous AHL.

CAT Oscillator (Figure 2.1A) is identical to the Stricker (2008) oscillator with the addition of a cassette containing ssrA-tagged CAT behind the hybrid lac/ara-1 promoter. As CAT is behind the identical promoter as GFP, GFP acts as a reporter for CAT expression in the CAT Oscillator. The Control Oscillator (Figure 2.1B) is identical to the Stricker (2008) oscillator with the addition of a cassette containing ssrA-tagged CAT behind the LuxI promoter. LuxR is a constitutively expressed protein in *E. coli* that, upon binding an N-Acyl homoserine lactone (AHL), will initiate transcription of genes downstream of the LuxI promoter. As such, in the case of the Control Oscillator, CAT expression is non-oscillatory and tunable with exogenously supplied AHL. In the original 2008 study, Stricker *et al.* showed that period of their synthetic oscillator was tunable by altering concentrations of either arabinose or IPTG in the cell media. In this study all experiments for both the CAT and Control Oscillator were generated using media containing 0.7% arabinose and 2 mM IPTG.

Chloramphenicol Sensitivity

In order to compare the entrainment dynamics of the CAT and Control Oscillator, it was necessary to determine a level of AHL at which these two oscillators are equally sensitive to chloramphenicol. Cells were seeded into a microfluidic device that forces cells to grow in a monolayer (Figure 2.2). Upon reaching confluency within the cell chambers, monolayers of cells were exposed to 340 μg/mL chloramphenicol for 12 hours at varying concentrations of AHL

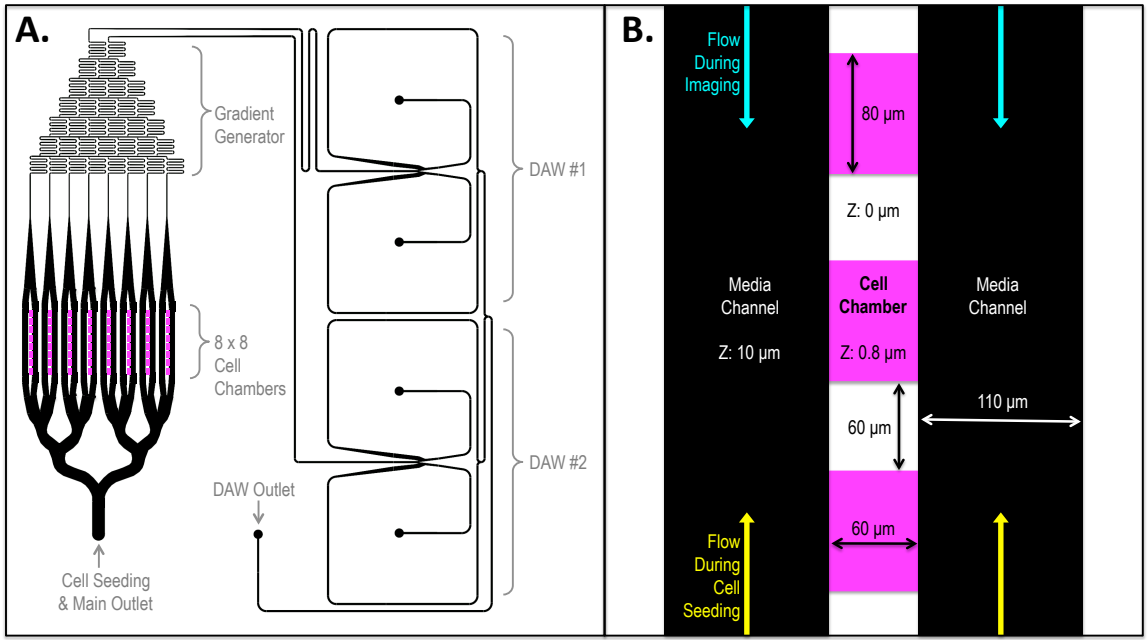

Figure 2.2: Microfluidic device for a gradient of dynamic conditions. A) Microfluidic device design containing a classic gradient generator in which each input is linked to a separate "Dial-a-Wave" (DAW) feature (for full description of the "Dial-a-Wave" feature refer to page 9). This device contains 8 x 8 chambers for growth of *E. coli* monolayers and allows for cells to be seeded and grown to confluency in the absence of chloramphenicol. It also allows for perfusion of a linear gradient of 8 dynamic media conditions. B) Specifications of cell chambers and media perfusion channels. Cell chambers are open on two ends to the perfusion channels allowing for cells and waste products to flush out and nutrients to diffuse in from both sides.

ranging from zero to 70 nM. 340 µg/mL chloramphenicol was chosen as it is not lethal, but causes decreased growth rate for CAT Oscillator cells (Figure 2.3). Brightfield images of the cells were captured every 2 minutes. These image sequences were then analyzed to determine the average number of division events/cell for each hour of chloramphenicol exposure. AHL concentration did not effect chloramphenicol sensitivity in the CAT Oscillator cells (Figure 2.4A). As expected, the Control Oscillator showed increased resistance to chloramphenicol with increased concentration of AHL (Figure 2.4B). In the absence of AHL the Control Oscillator did not divide at all. At concentrations of 10, 20 and 30 nM AHL the Control Oscillator initially was able to grow, but accumulated fatal chloramphenicol toxicity during the incubation. Altogether Figures 2.4A and 2.4B show that AHL concentrations of 30 nM and below caused the Control Oscillator cells to be more sensitive to chloramphenicol than the CAT Oscillator cells. AHL concentrations of 40 nM AHL to 70 nM caused equal chloramphenicol sensitivity between the two strains.

We next compared the CAT and Control Oscillator in an environment with oscillated chloramphenicol. We examined the Control Oscillator at levels of AHL causing equal (40 nM) and increased sensitivity to chloramphenicol (20 nM) as compared to the CAT Oscillator. Confluent monolayers of CAT and Control Oscillator cells were exposed to a continuously repeating 50-minute square wave of chloramphenicol (repetitions of: 25 minutes of no chloramphenicol, followed by 25 minutes of chloramphenicol). Chloramphenicol amplitudes ranged between

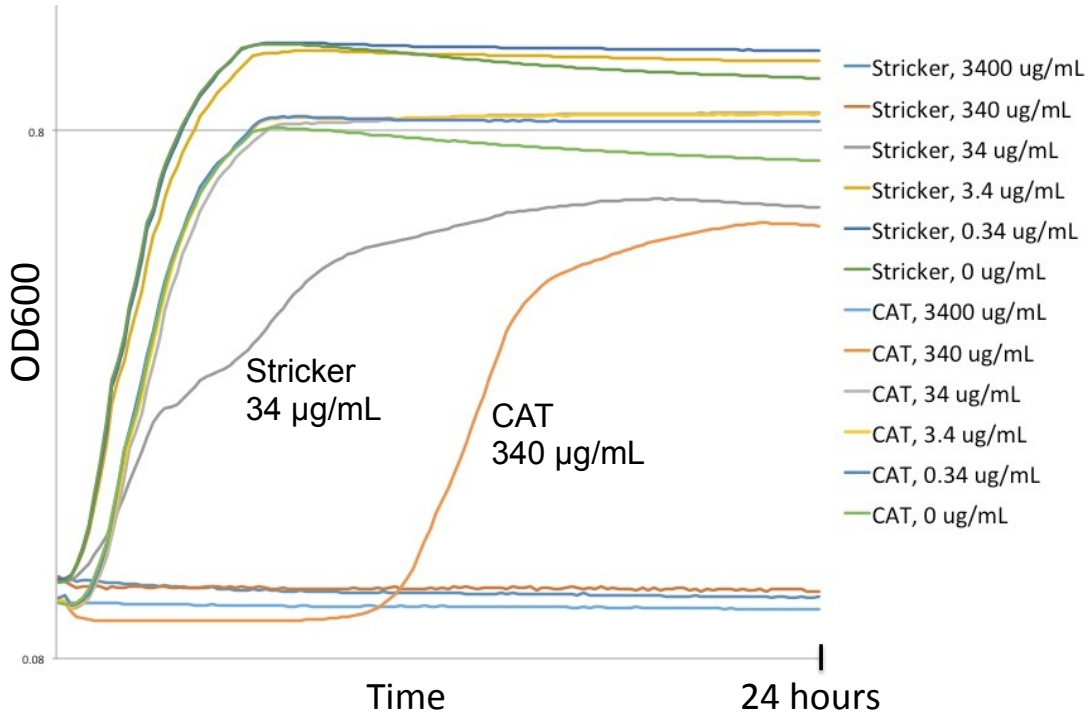

Figure 2.3: Chloramphenicol sensitivity in off-chip liquid culture. Standard 96-well plate growth curves for the 2008 Stricker Oscillator and the CAT Oscillator grown in a range of chloramphenicol concentrations where the y-axis is OD600 (log scale) and the x-axis is time (24 hours total).

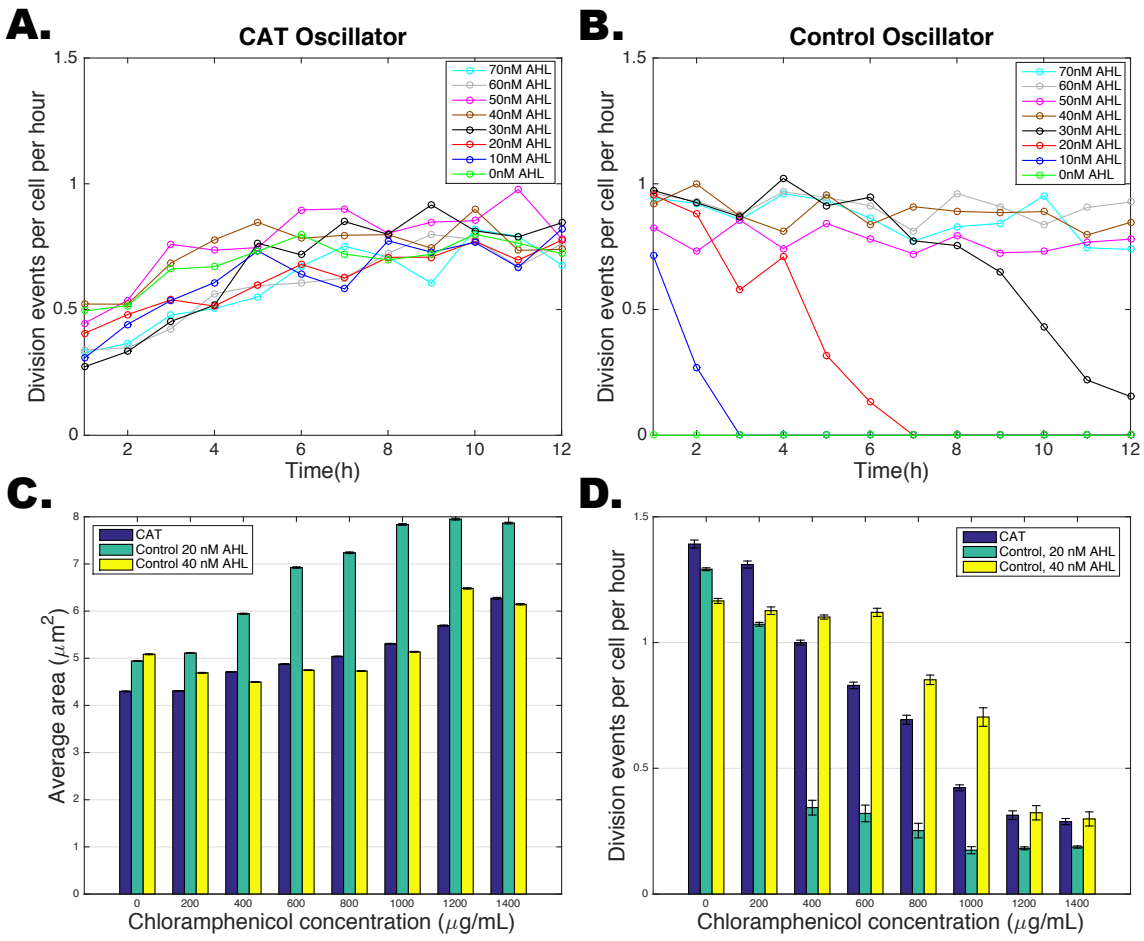

Figure 2.4: Chloramphenicol sensitivity of microfluidic monolayers. A & B) Chloramphenicol sensitivity in the A) CAT vs. B) Control Oscillator when grown in a range of AHL concentrations and non-oscillatory 340 µg/mL chloramphenicol as measured by average division events per cell per hour. C) Average area per cell after being grown in a 50-minute period square wave of a range of chloramphenicol amplitudes. Chloramphenicol toxicity is known to cause cell elongation and overall cell area enlargement. D) Average division events per cell per hour after being grown in a 50-minute period square wave of a range of chloramphenicol amplitudes.

zero and 1400 µg/mL. Brightfield images were captured every 2 minutes for 10 hours with continuous 50 minute period chloramphenicol oscillations. Chloramphenicol toxicity in *E. coli* is known to cause enlarged or "swollen" cells (Bergersen 1953, Morgan 1967). As such, we analyzed these images for both average cell area (Figure 2.4C) and also average division events/cell/hour (Figure 2.4D). By both metrics the Control Oscillator at 20 nM AHL is significantly more sensitive to oscillated chloramphenicol than the CAT Oscillator. The Control Oscillator at 40 nM AHL and the CAT Oscillator showed similar cell area and division phenotypes across the range of chloramphenicol amplitudes.

Chloramphenicol Entrainment Dynamics

Monolayers of CAT and Control Oscillator cells were imaged in the absence of chloramphenicol in order to examine the distribution of free-running GFP oscillatory periods for individual cells. The average free-running GFP period for the CAT Oscillator was found to be 40.85 minutes ± 1.71 and the Control Oscillator to be 43.38 minutes ± 2.16 (Figures 2.5B and C, "Free Oscillations"). Confluent monolayers of CAT and Control Oscillator cells (at 40 nM AHL) were then imaged during a continuously repeating 50 minute square wave of chloramphenicol (25 minutes of no chloramphenicol, followed by 25 minutes of 120 µg/mL chloramphenicol) for 10 hours. A rhodamine dye was added to the chloramphenicol media in order to track the timing of the chloramphenicol oscillations. GFP and rhodamine fluorescence images were

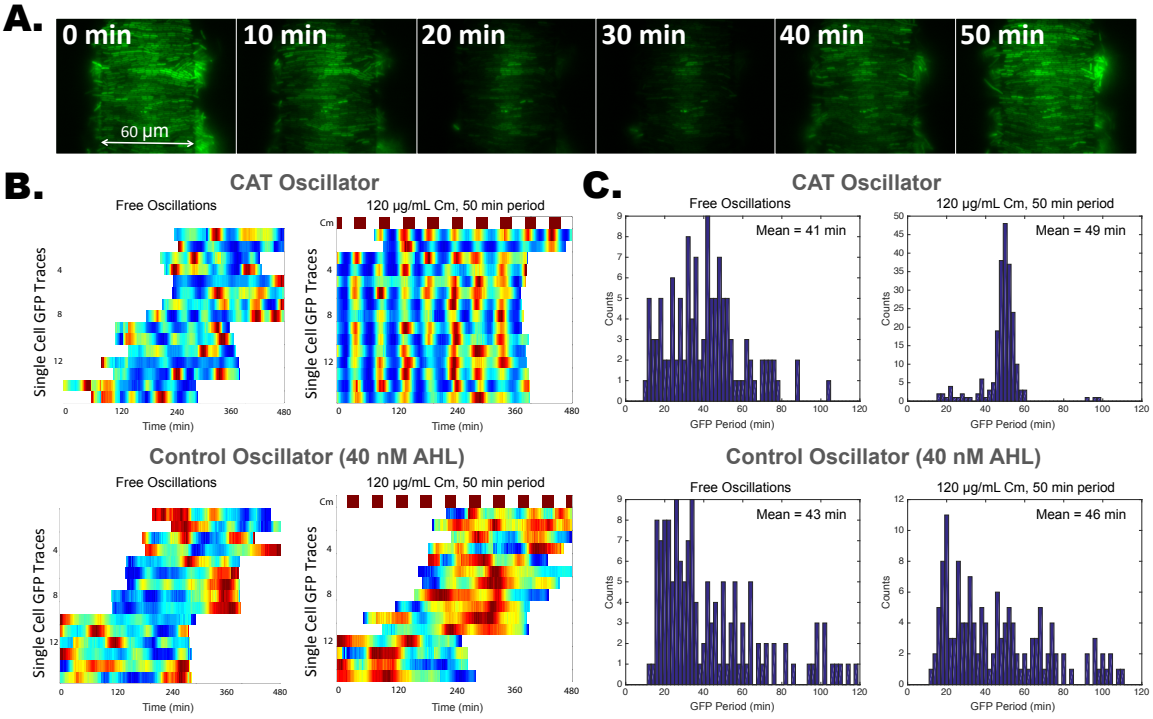

Figure 2.5: Single cell analysis of Cm entrainment for CAT vs. Control. A) Representative GFP fluorescence images of a monolayer of CAT Oscillator cells entrained to a 50-minute period square wave of 120 µg/mL chloramphenicol. 10 minutes elapsed between each successive image. B) Representative single cell GFP trace heat maps for cells grown either in free-running conditions or in a 50-minute period square wave of 120 µg/mL chloramphenicol for the CAT Oscillator versus the Control Oscillator induced with 40 nM AHL. C) Histograms displaying the distribution of GFP periods for cells grown either in free-running conditions or in a 50 minute period square wave of 120 µg/mL Cm for the CAT Oscillator versus the Control Oscillator induced with 40 nM AHL.

captured every 2 minutes. Images were analyzed to obtain GFP fluorescence traces from individual cells. Nearly all CAT Oscillator cells adjusted their phase and period to match that of the environmental chloramphenicol (Figure 2.5A, B and C). The distribution of GFP periods for the individual CAT Oscillator cells dramatically narrowed in response to the chloramphenicol oscillations. The distribution of GFP periods for the individual Control Oscillator cells did not significantly change due to the chloramphenicol oscillations (Figure 2.5B and C).

To characterize the entrainment behavior of the CAT and Control Oscillator strains across different signal amplitudes and periods, we extracted a number between 0 and 1 that quantified the prevalence of the drive frequency in the median fluorescence signal from an entire 60 μm(X) x 80 μm(Y) x 0.8 μm(Z) cell chamber (see Methods for details). If cells were desynchronized, we expected the median fluorescence in the trap to fluctuate stochastically, whereas a perfectly entrained population would lead to a periodic median fluorescence signal that had the same frequency as the drive. We found this easily computed “bulk entrainment” measure (Figure 2.6) to yield significantly more robust results than more traditional order parameters that rely on the phase of individual oscillators computed from noisy fluorescence signals of single cells.

For a 50 minute drive period with chloramphenicol amplitudes ranging from 0 to 140 μg/ml, bulk entrainment of the CAT Oscillator was substantially higher compared to that of the Control Oscillator at 40 nM AHL induction (Figure

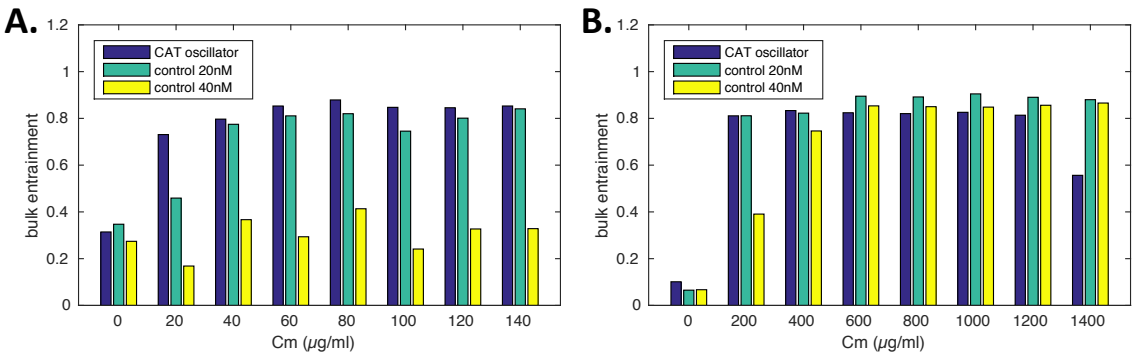

Figure 2.6: Bulk analysis of Cm entrainment for CAT vs. Control. Degree of GFP entrainment for the CAT versus Control Oscillator using median cell chamber fluorescence. CAT and Control cells were grown in a 50-minute period chloramphenicol square wave with a range of amplitudes: A) Linear gradient from zero to 140 μg/ml. B) Linear gradient from zero to 1400 μg/ml.

2.6A). Only much higher concentrations of chloramphenicol were able to entrain the Control Oscillator at 40nM AHL (Figure 2.6B). Even under 20 nM induction conditions, which we have shown to result in significantly greater chloramphenicol sensitivity (Figure 2.4), bulk entrainment of the CAT Oscillator was still stronger than the Control strain (Figure 2.6A).

A full scan of chloramphenicol periods and amplitudes for the CAT Oscillator revealed that CAT Oscillator cells are entrained most easily at a 50 minute drive period (Figure 2.7B), which is slightly longer than the free-running period and corresponds to a classical Arnold tongue for 1:1 entrainment. Towards shorter periods, the chloramphenicol signal quickly looses efficiency in entraining the oscillator for any tested drive amplitude, whereas longer drive periods are generally able to entrain the oscillator at some window of amplitudes. Bulk entrainment analysis (Figure 2.7B) also hints at a second more efficient drive period of around 90 minutes which would correspond to 1:2 entrainment.

We noticed systematic differences in the position of the GFP peak with respect to the “ON” phases of the chloramphenicol signal for different drive periods (Figure 2.8A). To quantify this effect, we also analyzed the phase shift of the median fluorescence signal in the trap for drive parameters that yielded bulk entrainment greater than 0.6 (Figure 2.8B). The phase shift increases gradually with the drive period, corresponding to an increasingly earlier onset of the GFP signal with respect the onset of the next chloramphenicol pulse. This is

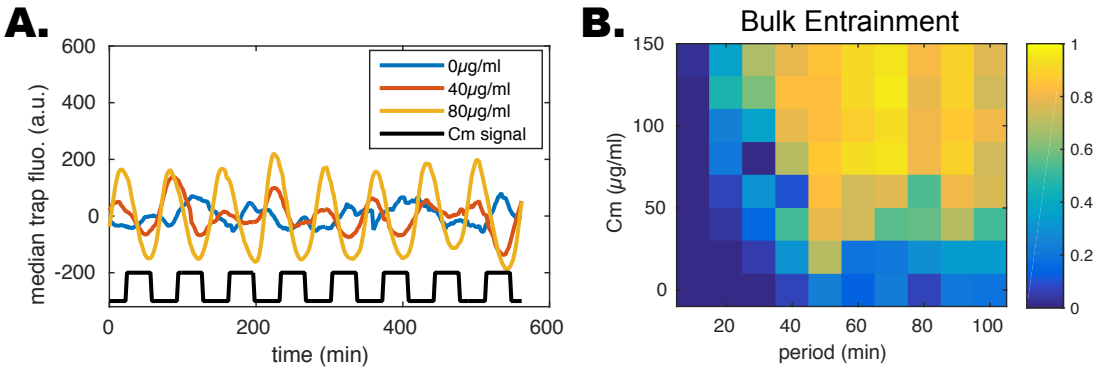

Figure 2.7: Bulk entrainment dynamics of the CAT Oscillator. A) Mean fluorescence for a trap of CAT Oscillator cells grown in a 70-minute Cm square wave of varying amplitudes. B) Heat map showing extent of CAT Oscillator bulk entrainment across a matrix of chloramphenicol drive periods and amplitudes.

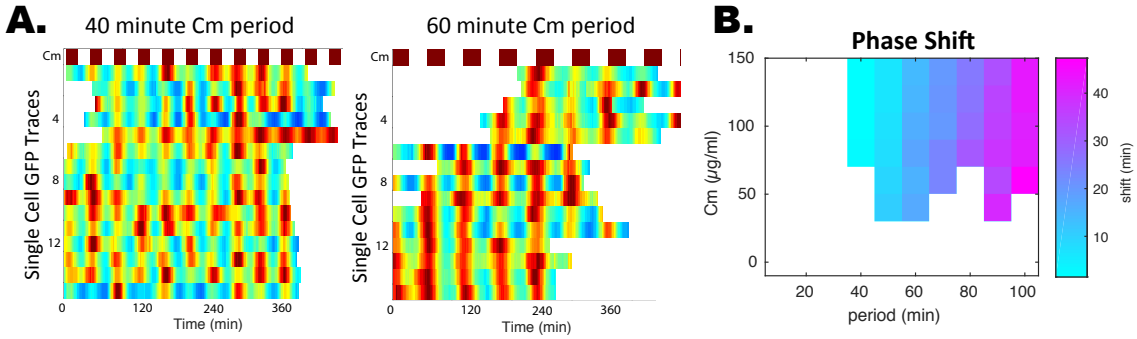

Figure 2.8: CAT Oscillator phase shift analysis. A) Representative single cell GFP fluorescence traces for CAT Oscillator cells entrained to a 40 vs. 60-minute period Cm drive. B) Heat map showing degree (in minutes) of phase shift with regard to the alignment of peak GFP fluorescence with the Cm drive "ON" time.

consistent with the simple picture where chloramphenicol – during the preceding ON phase – inhibits protein production once CAT has been sufficiently degraded inside the cell and the next oscillation is started once chloramphenicol is removed from the medium. Because there is more time in between chloramphenicol ON phases as the period increases, GFP peaks earlier before the next ON phase. This hypothesis is also in agreement with rapid loss of entrainment towards shorter drive periods (Figure 2.7B), because the windows for chloramphenicol to interact with the oscillator might not be sufficiently long in this regime. Examining GFP periods of individual cells across the matrix of chloramphenicol periods and amplitudes uncovered bi and tri-modal distribution patterns at shorter chloramphenicol drive frequencies (Figure 2.9). This shows that, despite bulk entrainment being low at these frequencies, there is still a form of interaction between the CAT Oscillator and the chloramphenicol environment.

Proposed Mechanism

Through comparison to the Control Oscillator, we have shown that CAT Oscillator entrainment at low drive amplitudes involves something other than the simple turning on and off of translation by chloramphenicol. If the CAT Oscillator becomes out of phase with its chloromphenicol environment, this would theoretically cause CAT to be expressed when chloramphenicol is not present. CAT expression would then turn off at a time when chloramphenicol is present. Without CAT, we hypothesize that the chloramphenicol could cause the

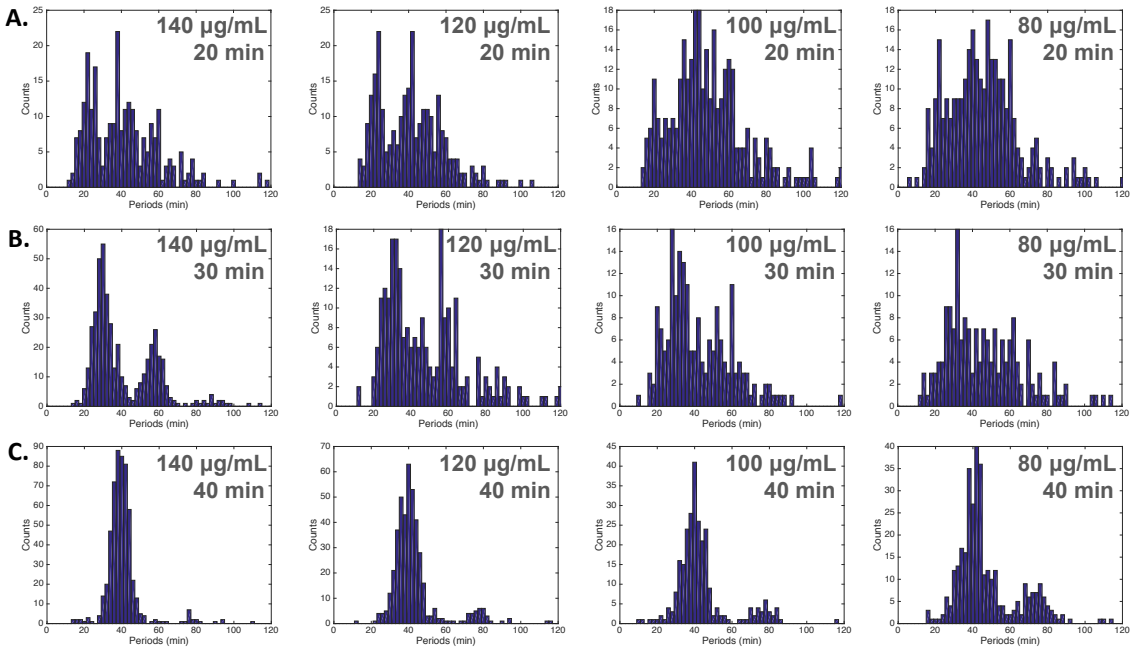

Figure 2.9: Multi-modal entrainment dynamics. GFP oscillatory period distributions for the CAT Oscillator in response to a A) 20, B) 30, and C) 40-minute chloramphenicol drive. These show the emergence of trimodal and bimodal GFP period distributions at lower frequency chloramphenicol drives.

oscillatory machinery to subtly slow in such a way that does not noticeably effect growth rate, but does result in a slightly extended "CAT off" period. This extended “CAT off” period could allow the oscillator to synch back up with the oscillating chloramphenicol drive after several generations. Our group has previously shown that the phase of the Stricker (2008) oscillator is heritable for multiple cell cycles. Thus, once a CAT Oscillator cell is in sync with its chloramphenicol environment, that cell lineage will stay in sync for several generations. If a cell were to become critically out of sync with a chloramphenicol drive, this cell would die and make room for more fit cell lineages. If our proposed mechanism is accurate, the “phenotypic entrainment” that we have witnessed is caused by a subtle fitness advantage conferred by the alignment of CAT Expression with its chloramphenicol environment.

In the data we have presented here, there is a clear drive amplitude window where the CAT oscillator will out-entrain the Control Oscillator. Several studies have been published in which a synthetic oscillator has been entrained through a direct molecular interaction between the environment and the synthetic circuitry. Entrainment through an engineered fitness advantage conferred by an oscillated protein product - to our knowledge - was uncharted territory prior to this study. As a pair, CAT and chloramphenicol are merely a somewhat brute-force jumping off point to studying this form of entrainment. To further understand this phenomenon more subtle forms of oscillated fitness advantage should be examined.

2.4 Methods Summary

Plasmids, Strains and Media

The plasmids used in this study were either purchased from www.transcriptic.com or constructed using a basic CPEC PCR-based cloning strategy with pre-existing genetic parts. The CAT and Control Oscillator strains were constructed by transforming either 2 or 3 (respectively) plasmids into JS006 *E. coli* competent cells. The JS006 strain is MG1655 ΔaraC ΔlacI and was originally constructed by Stricker *et al.* (2008). Transformed cells exhibiting the proper drug resistance were cloned and subsequently sequenced to verify proper circuit construction. Basic LB Broth containing 0.075% Tween 20 (to prevent clogging within microfluidic devices) was used for all experiments. Antibiotics for selection were included in the media for all experiments (Kanamycin and Ampicillin for CAT; Kanamycin, Ampicillin and Spectinomycin for Control). Media for all experiments for both the CAT and Control Oscillator also contained 0.7% arabinose and 2 mM IPTG. The specific AHL used in this study was: 3-oxo-C6-HSL. Sulforhodamine 101 fluorescent dye was added to media containing chloramphenicol as a marker for the chloramphenicol oscillations.

Microfluidic Devices and Microscopy

The exact design and specifications of the microfluidic device used in this study can be found in the supplementary information (Figure 2.2). Microfluidic devices were fabricated by first creating a multilayer master-mold using

photolithography. SU-8 negative photoresists (Microchem Corporation) were used to create the master-mold according to manufacturer protocols. The devices were then made by pouring and curing polydimethyl-siloxane (PDMS) onto the master-mold. PDMS was prepared by mixing Sylgard 184 Elastomer curing agent and base (DOW Corning) in 1:10 ratio. PDMS was poured onto the master-mold, degassesd for 30 min, cured for 1 h at 80°C, and then carefully peeled off the mold. Port holes were punched using a 0.5 mm Harris Uni-Core hole puncher (Ted Pella, Inc.) and the devices were subsequently bonded to glass coverslips (Corning) via oxygen plasma exposure (Jelight UVO cleaner Model no. 42, 0.6 scfm O_2, 3 min). Acquisition of images was performed at 37°C with a Nikon TI2 Microscope using a Photometrics CoolSnap cooled CCD camera. The microscope and accessories were programmed using the Nikon Elements software. For all experiments, images were captured every 2 minutes.

Prior to setting up an experiment, overnight bacterial cultures were diluted 1:100 and incubated at 37°C for 2 hours. After 2 hours, 1 mL of the 1:100 dilution was spun down at 3000 RCF for 3 minutes. Supernatant was then removed and the cell pellet was resuspended in 40 uL of fresh media. Media for the various experimental conditions was loaded into open (plunger-free) 60 mL syringes attached to tygon tubing. In order to load cells into the microfluidic chambers and fully wet the microfluidic device, devices were treated in a vacuum chamber for 20 minutes (Edwards RV3 vacuum pump at 29.5 inches Hg below room pressure). Directly after being removed from the vacuum chamber, 2 µL of

the resuspended cell pellet was pipetted onto the “Cell Seeding” port of the device (Figure 2.2). 2 µL of blue food coloring (for visible wetting) was pipetted onto all other ports. Due to the prior vacuum treatment, fluid pipetted onto the ports was pulled into the device until the device channels were fully wetted and void of any bubbles (see Liang 2011 for a full description of degass driven loading of a PDMS-based microfluidic device). Once the cell suspension visibly met the blue food coloring within the device (indicating full device wetting) tygon tubing from the prepared syringes was connected to the ports via metal connectors. For all experiments, seeded cells were grown in the absence of chloramphenicol until cells reached confluency within the microfluidic cell chambers and imaging was started.

Single Cell Tracking

To obtain and analyze single cell data from time lapse images, we adopted a recently developed single cell tracking algorithm (Mondragón-Palomino 2011). Once single cell objects were identified, the tracking algorithm described previously was applied to obtain single cell time course information about the area and mean fluorescence of the cells. By identifying large drops in single cell area trajectories we were able to detect division events. Division events per cell per hour were calculated as following: for each time-lapse image, we obtained the number of cells in the trap and averaged the number of cells in one hour (30 images in total, because images were taken every 2 minutes) to get

the average cell number per hour. Then, the division events per cell per hour were calculated by dividing the total division events in each hour by the average cell number per hour.

In the Figure 4 bar graphs, the average area under each chloramphenicol concentration was calculated as following: first, the average cell area was calculated for each time-lapse image. Then these average cell areas per image were averaged among 30 images in one hour. The average cell areas per hour were then averaged in the whole experiment to get the total average area with standard error indicated by the error bar. Division events per cell per hour were also calculated by averaging the division events per cell per hour among all hours in the whole experiment with standard error indicated by the error bar. In the heat maps, the fluorescence intensity in each trace was normalized from 0 to 1 the get the relative fluorescence intensity.

Bulk Entrainment and Phase Shift Analysis

The median fluorescence intensity from the entire trap is calculated and a moving average with a window length of 200 minutes is subtracted to account for signal drift. The power spectrum of the resulting time series is obtained using a discrete Fourier transform (DFT). Bulk entrainment is defined as the power, Pd, concentrated around the drive frequency divided by the total power of the signal Pt. Pd is calculated as the sum of the frequency component closest to the drive frequency and the two adjacent frequency components to account for possible

clock inaccuracies ($0.084h^{-1}$ to $0.108h^{-1}$ away from the expected frequency depending on the length of the time trace). The phase difference is obtained by comparing the complex phase angle of the DFT component closest to the drive frequency to the phase angle of the same component for the chloramphenicol signal. This phase difference is then converted to minutes using the drive period.

2.5 Acknowledgments

The work presented in this chapter was a collaboration between Megan Dueck (primary researcher and author), Philip Bittihn (assistance with mathematical analysis), Liyang Xiong (assistance with single cell tracking), Lev Tsimring (faculty mentor) and Jeff Hasty (faculty mentor).

2.6 References

Atkinson MR, Savageau MA, Myers JT, Ninfa AJ (2003) Development of genetic circuitry exhibiting toggle switch or oscillatory behavior in *Escherichia coli*. Cell 113(5):597-607.

Bergersen FJ (1953) Cytological changes induced in *Bacterium coli* by chloramphenicol. J. Gen. Microbiol. 9:353-356.

Chen Y, Kim JK, Hirning AJ, Josić K, Bennett MR (2015) Emergent genetic oscillations in a synthetic microbial consortium. Science 349(6251):986-9.

Danino T, Mondragón-Palomino O, Tsimring L, Hasty J (2010) A synchronized quorum of genetic clocks. Nature 463(7279):326-30.

Dies M, Galera-Laporta L, Garcia-Ojalvo J (2016) Mutual regulation causes co-entrainment between a synthetic oscillator and the bacterial cell cycle. Integr Biol (Camb) 8(4):533-41.

Elowitz MB, Leibler S (2000) A synthetic oscillatory network of transcriptional regulators. Nature 403(6767):335-8.

Franco E, Friedrichs E, Kim J, Jungmann R, Murray R, Winfree E, Simmel FC (2011) Timing molecular motion and production with a synthetic transcriptional clock. Proc Natl Acad Sci U S A. 108(40):E784-93.

Fung E, Wong WW, Suen JK, Bulter T, Lee SG, Liao JC (2005) A synthetic gene-metabolic oscillator. Nature 435(7038):118-22.

Hussain F, Gupta C, Hirning AJ, Ott W, Matthews KS, Josic K, Bennett MR (2014) Engineered temperature compensation in a synthetic genetic clock. Proc Natl Acad Sci U S A. 111(3):972-7.

Kim J, Winfree E (2011) Synthetic *in vitro* transcriptional oscillators. Mol Syst Biol 7:465.

Liang DY, Tentori AM, Dimov IK, Lee LP (2011) Systematic characterization of degas-driven flow for poly(dimethylsiloxane) microfluidic devices. Biomicrofluidics 5(2):24108.

Lutz R, Bujard H (1997) Independent and tight regulation of transcriptional units in *Escherichia coli* via the LacR/O, the TetR/O and AraC/I1-I2 regulatory elements. Nucleic Acids Res. 25, 1203–1210.

Mondragón-Palomino O, Danino T, Selimkhanov J, Tsimring L, Hasty J (2011) Entrainment of a population of synthetic genetic oscillators. Science 333(6047):1315-9.

Morgan C, Rosenkranz HS, Carr HS, Rose HM (1967) Electron microscopy of chloramphenicol treated *Escherichia coli*. J. Bacteriol. 93:1987-2002.

Ouyang Y, Andersson CR, Kondo T, Golden SS, Johnson CH (1998) Resonating circadian clocks enhance fitness in cyanobacteria. Proc Natl Acad Sci U S A. 95(15):8660-4.

Prindle A, Samayoa P, Razinkov I, Danino T, Tsimring LS, Hasty J (2011) A sensing array of radically coupled genetic 'biopixels'. Nature 481(7379):39-44.

Prindle A, Selimkhanov J, Li H, Razinkov I, Tsimring LS, Hasty J (2014) Rapid and tunable post-translational coupling of genetic circuits. Nature 508(7496):387-91.

Ryback BM, Odoni DI, van Heck RG, van Nuland Y, Hesselman MC, Martins Dos Santos VA1, van Passel MW, Hugenholtz F (2013) Design and analysis of a tunable synchronized oscillator. J Biol Eng. 7(1):26.

Sowa SW, Baldea M, Contreras LM (2014) Optimizing metabolite production using periodic oscillations. PLoS Comput Biol. 10(6):e1003658.

Stricker J, Cookson S, Bennett MR, Mather WH, Tsimring LS, Hasty J (2008) A fast, robust and tunable synthetic gene oscillator. Nature 456(7221):516-9.

Chapter 3: A Massively Parallel Microfluidic Device for Long-Term Visualization of Isolated Motile Cells

3.1 Abstract

Visualizing the natural behavior of motile cells over many hours is a challenge, as cells can leave the field of view of a microscope in a matter of minutes. Many interesting cell behaviors—such as cell division, motility phenotype, cell–cell interactions, and multicellular colony formation—require hours of observation to characterize. We present a microfluidic device that traps hundreds of single motile cells in isolated chambers, thereby allowing observation over several days. This polydimethylsiloxane device features 400 circular chambers, connected to a central serpentine channel. Motile cells are loaded into these chambers through the serpentine channel. After complete device wetting the channel is purged with air, fluidically isolating the chambers from each other and effectively trapping the cells. We applied the device to observe the behavior and motility phenotypes of the choanoflagellate *Salpingoeca rosetta*. Because of its ability to live in both solitary and colonial forms, *S. rosetta* is a useful model organism for the study of the evolutionary origins of multicellularity. In particular, *S. rosetta* can take on two distinct colonial forms: chain colonies and rosette colonies. With our device, we are able to observe the formation of these colonies from single cells more easily and with higher throughput than ever before. This device has the potential to be a powerful tool for studying the long-term behavior of motile cells.

3.2 Introduction

Microfluidic biological assays allow investigators to address biological questions which are difficult to answer with conventional techniques. With microfluidic trapping technologies, single-cell assays can be performed in a high-throughput manner using limited reagents (Breslauer *et al*. 2006; Ingham and Vlieg 2008; Kim *et al*. 2008; Muralimohan *et al*. 2009; Nilsson *et al*. 2009; Weibel *et al*. 2007; Di Carlo and Lee 2006). Along with this advantage, microfluidic has also made it possible to grow cells indefinitely within a chemostat (Balaban 2005; Groisman *et al*. 2005; Novick and Szilard 1950), study cellular chemotaxis with a steady-state concentration gradient (Mao *et al*. 2003), and allow cell sorting and sample dispensing all on one chip (Fu *et al*. 2002), to name a few examples.

The choanoflagellate *Salpingoeca rosetta* is a flagellated protozoan whose study would greatly benefit from an effective microfluidic isolation device. Choanoflagellates are the closest known extant relatives of metazoans (Fairclough *et al*. 2010; King 2004, 2005; Lang *et al*. 2002). S. rosetta is a unique model organism for studying the evolution of multicellularity because it can exist either solitarily or in one of two colonial forms, chain or rosette, depending on environmental cues (Alegado *et al*. 2012; Fairclough *et al*. 2010). Visualizing the formation of *S. rosetta* colonies from a single cell using conventional techniques is an extremely time-consuming and challenging task, as it requires constant tracking of the cells for at least 12 h. Furthermore, it is difficult to track more than one cell/colony at a time. Long-term visualization would be more accessible with

the aid of a high-throughput microfluidic device that could isolate single cells within one microscopic field of view without hindering their movement.

Designing such an isolation device presents several challenges. Most microfluidic devices for single-cell analysis are designed for adherent cells with limited motility. Motile cells, such as choanoflagellates, are capable of escaping most device traps. Microwells, for example, are effective with adherent cells for a wide range of applications (Lindstrom and Andersson-Svahn 2010, 2011) including studying the dynamics of stem cell differentiation (Lindstrom *et al*. 2009a), massively multiplexed PCR genotyping (Lindstrom *et al*. 2009b), and protein-binding assays (Friedman *et al*. 2009); however, microwells cannot confine cells in 3D, and so motile cells can simply swim out of the chambers (Lindstrom and Andersson-Svahn 2011). Another common method for studying non-motile cells is a mechanical trap, which confines cells with a variety of different physical structures. Examples of the diverse techniques developed for mechanical traps include using magnetic force to immobilize cells into an array (Liu *et al*. 2009), capturing large cells by filtering cell solution through a membrane microfilter (Zheng *et al*. 2007), and trapping single cells within U-shaped structures (Di Carlo *et al*. 2006). However, even if these traps could be adapted for use with motile cells, they ultimately immobilize the cells, thereby preventing the study of their natural movement and behavior. The few devices that have been specifically designed for motile cells similarly immobilize the cells using hydrodynamic trapping (Kumano *et al*. 2012; Lutz *et al*. 2006), likewise

rendering these devices inadequate for studying cell motility, growth, or developmental processes. Clearly, a need exists for a device that can be used for visualization of motile cells without hindering their movement or subjecting them to mechanical forces that may alter their behavior.

We present a microfluidic device that traps single motile *S. rosetta* cells in isolated chambers where cells can function normally and move freely. Each chamber serves as a miniaturized suspension cell culture for the isolated motile cells. The cells can be visualized for over 65 h as they divide, form colonies, and interact with other daughter cells. The design is both simple to fabricate and simple to operate. The chip consists of 400 circular chambers, branching off of a serpentine channel and can be self-loaded with the cell solution after vacuum treatment by degas-driven flow (Cira *et al*. 2012; Dimov *et al*. 2011; Luo *et al*. 2008). Degas-driven flow is a simple loading mechanism that is caused by the diffusion of air back into PDMS after the device has been ‘degassed’ in a vacuum. As the PDMS absorbs the air, this creates negative pressure inside the channels of the device, which draws the sample fluid into the isolation chambers. The chip can be vacuum-treated just prior to an experiment. Alternatively, if a vacuum system is unavailable in the laboratory, the chips can be pretreated with vacuum at the time of fabrication and hermetically sealed in plastic bags with an inexpensive food vacuum sealer. In that case, the bag is simply cut open and the chip immediately loaded with the cell solution. After loading the cell solution, the chambers are fluidically isolated by pumping air through the serpentine channel,

creating an air–fluid barrier that effectively traps the cells in the chambers. Surface tension at the narrow chamber opening prevents the media in the chambers from being flushed out during this process. Once the cells are confined, we can observe cell behavior, division, and colony formation on a massive scale unattainable with conventional techniques. Initial cell concentration can be adjusted to tune the final counts of cells/chamber.

Media retention, chamber size parameters, and cell media concentration have all been optimized for the study of *S. rosetta*, but can easily be modified for application to other types of motile organisms. This device provides a simple and high-throughput way to study the division and interaction of motile microorganisms through long-term visualization.

3.3 Methods

Device Fabrication

We fabricated the microfluidic device using standard soft lithography (Xia *et al*. 1999). A 50-μm single-layer negative mold was photolithographically patterned with SU-8 photoresist. Polydimethylsiloxane (PDMS, Sylgard 184), mixed at a 10:1 elastomer-to-curing-agent ratio, was poured over the mold and allowed to cure for 4 h at 60 °C. PDMS devices were bonded to a glass slide via oxygen plasma treatment. The devices included 400 trapping chambers, 70 μm in radius, connected to a 60-μm-wide serpentine channel via media retention bridges, 70 μm long and 25 μm wide (Fig. 3.1).

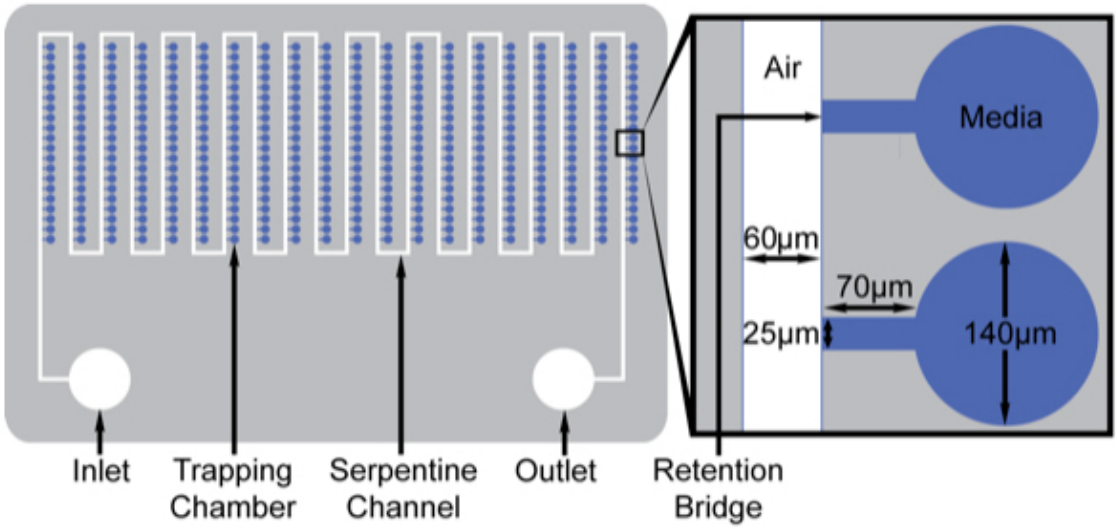

Figure 3.1: Microfluidic Device Schematic. The device consists of 400 trapping chambers branching from a serpentine channel. Narrow retention bridges between the chambers and the serpentine channel decrease media loss in the circular viewing chambers. Air is pumped through the serpentine channel to achieve fluidic isolation of each chamber.

Microfluidic device operation

The choanoflagellate suspension was loaded via degas-driven flow, and the chambers were then isolated by flowing air through the serpentine channel (Fig. 3.2). First, we placed the device in a vacuum chamber for ten min at ~300 mTorr with the outlet hole covered with Scotch tape (3 M). After removing the device from the vacuum, 20 µL of cell suspension was placed on the inlet. After 30 min, media had entirely filled the chambers, and cells were distributed among the chambers. We removed the tape covering the outlet and inserted a stainless steel catheter into the outlet hole. A 10-mL syringe on a syringe pump (New Era Pump Systems) was connected with tubing to the inlet hole of the device with a stainless steel catheter. Since PDMS is permeable to water vapor, the device was completely submerged in a petri dish filled with deionized water to prevent media evaporation from the chambers. The syringe pump pumped air through the device at 10 mL/h until the loading channel had been evacuated. Once the loading channel was evacuated, the syringe pump was set to 0.1 mL/h for the remainder of the study. This constant airflow provided necessary oxygen transport to support cell viability.

Cell culture

The choanoflagellate cell line *S. rosetta* (ATCC) with *E. pacifica* bacteria was cultivated in cereal grass media, which is processed by steeping artificial sea water in Ward's cereal grass (Scholar Chemistry), followed by filter sterilizing. Cells were grown at room temperature and subcultured every day.

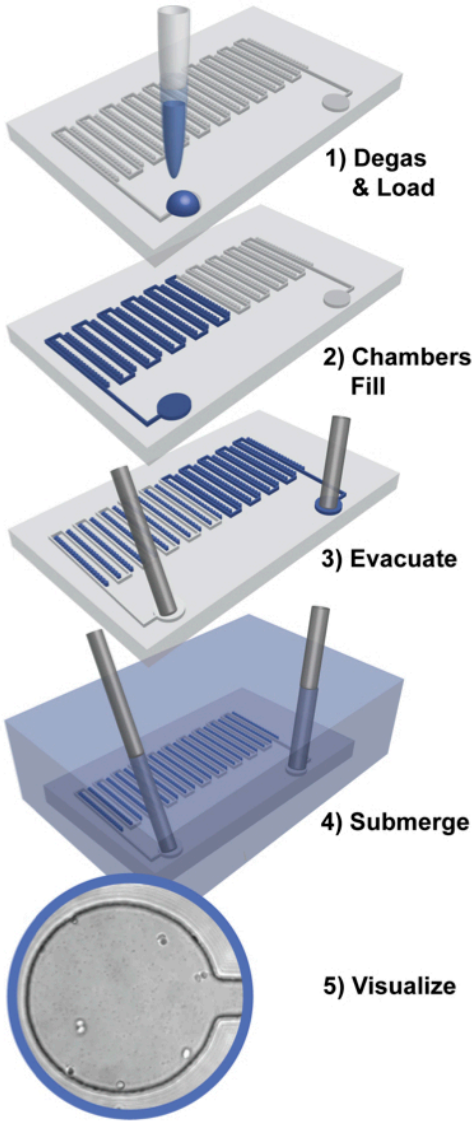

Figure 3.2: Microfluidic Device Operation. To operate, the device is degassed in a vacuum chamber for 5 min (1). After removal from the vacuum chamber, a drop of cell solution is loaded on the inlet, which fills all the chambers (2). Next, a syringe pump flows air through the device evacuating the serpentine channel and effectively trapping the cells in the chambers (3). Finally, the device is submerged in water to retain media (4). Cells can then be visualized under a microscope (5).

In preparation for cell injection into the microfluidic chip, cells were subcultured daily at a 1:5 cell-to-media concentration to progress the cells into log-phase growth. We concentrated the cells by centrifugation, followed by aspiration of the media. To form rosette colonies, one colony of *A. machipongonensis* was added to the cells. Since the culture was still dominantly composed of single cells up to 18 h after induction, we waited approximately 12–18 h before loading the induced cells into the chip.

Visualization of cells on chip

Cells were visualized on the chip under phase-contrast microscopy. For long-term visualization of a small number of chambers, one field of view of the microscope was recorded for 24 h with images taken at 10-s intervals. For experiments involving many chambers, an automated stage was used to take pictures of each chamber in the device once per hour for 68 h. ImageJ was used to conduct particle tracking of the cells in the chambers, and MATLAB was used to process the data from ImageJ.

Media retention analysis

Media retention capabilities of submerged and non-submerged devices were examined with a fluorescence-based assay. After loading the devices with a 1 μM solution of green fluorescent protein (GFP) in deionized water, we submerged one device in a petri dish filled with water and left another device non-submerged. We evacuated the serpentine channels of the devices, leaving

GFP only inside the chambers, and imaged three consecutive rows of each device at 0, 3, 6, 12, and 24 h after evacuating the serpentine channel. The images were captured using an inverted epi-fluorescence microscope with a 40× objective magnification (Motic AE31). The cross-sectional area of media retained was determined across >20 chambers at each time point using ImageJ.

Chamber size comparison

Three different devices were fabricated with chambers of 30, 50, and 70 μm radii to investigate the effect of chamber size on the rate of proliferation of trapped cells. A cell suspension containing 2.5×10^6 cells/mL of media was injected into the chip and loaded into the three different devices simultaneously. Cell numbers were recorded in each chamber of five rows for each device at 0, 12, and 24 h after loading.

Trapping efficiency analysis

The distribution of the number of trapped cells per chamber given different initially loaded cell concentrations was analyzed. The device was loaded with four different concentrations of choanoflagellates in media, ranging from 100,000 cells/mL to 8.35 million cells/mL. To allow the cells to become more evenly distributed across the device, cells were allowed to move naturally for 30 min after loading the devices, before counting began. After the incubation, the number of cells in each trapping chamber from four rows of the device was analyzed and recorded.

3.4 Results and Discussion

Visualization of cells on chip

We were able to visualize the *S. rosetta* cells in the device under phase contrast for over 2 days as they moved throughout the chambers, interacted with each other, proliferated, and formed colonies.

Figure 3.3a shows a rosette colony that formed in the device from a single cell after induction with *A. machipongonensis* 18 h prior to loading. The image was captured 18 h after loading the device. Due to the extreme difficulty in using conventional methods to visualize motile cells, the formation of a rosette colony has been captured on video only once before (Fairclough *et al.* 2010). Our device has the potential to procure hundreds of recordings of rosette formations within a single experiment. Figure 3.3b demonstrates tracking of several choanoflagellates in a chamber over a period of 10 s. Such tracking can enable high-throughput studies of motility phenotype.

Using an automated stage, we captured data from many chambers over a 68-h period. We investigated colony formation of *S. rosetta* cells by recording the percentage of cells which formed colonies versus those that remained solitary based on the proximity of neighboring cells. Eleven chambers which had a single, healthy cell at the start of the experiment were selected for analysis. Cells which had a centroid spacing within 10 μm of one another were considered to be part of a colony; all others were considered solitary.

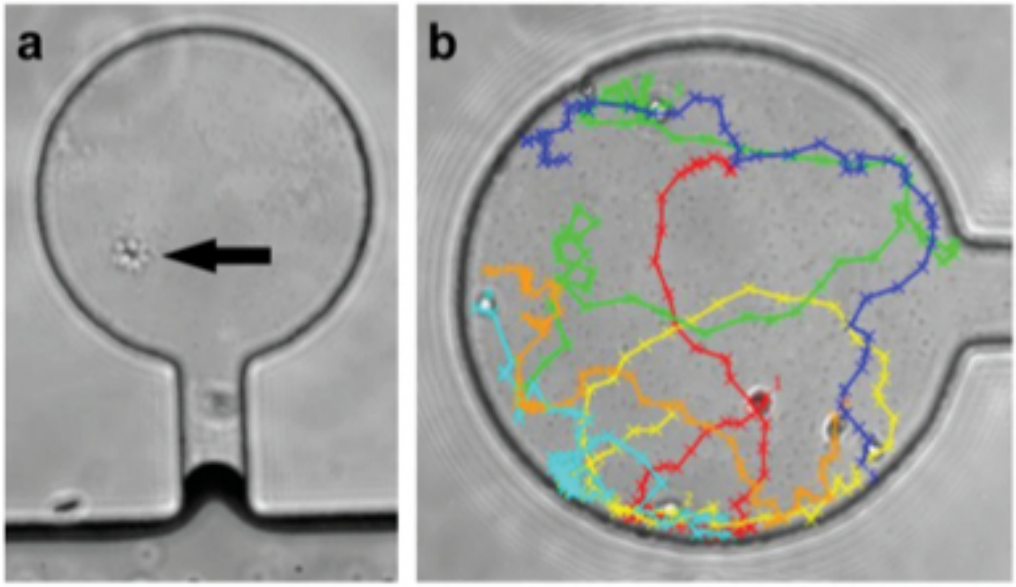

Figure 3.3: Tracking choanoflagellate behavior. a) Phase-contrast image of a rosette colony that formed in the device, starting from a single cell. b) This image shows the path of several choanoflagellates in an isolated chamber over a short period of time. Each 'x' represents the location of a cell after five frames of video (at 30 frames per second).

After 68 h, the average cells per chamber had grown from 1 cell to 6.9 cells, corresponding to a doubling time of 21.4 h, which is within the range of doubling times of 11–25 h seen in bulk culture conditions (Wain 2011; Fairclough *et al.* 2010). This indicates that the device does not adversely affect cell proliferation. Approximately 25 h into the experiment, the average number of cells per chamber reached two, and the percentage of solitary cells decreased below 20 % as the cells began forming chain colonies (Fig. 3.4a, b). As the colonies increased in size, cells began to bud off the colonies, resulting in an increase in the percentage of solitary cells approximately 45 h after loading (Fig. 3.4b, c). One possible explanation for this observation is that colony size is limited by mass transport of nutrients, so beyond a certain size, colonies tend to disaggregate. Figure 4d shows representative images of one chamber at different time points illustrating a single starting cell (3 h), a chain colony of three cells (31 h), partial disaggregation of this colony as it grows to five cells (45 h), and complete disaggregation with seven cells in the chamber (67 h).

Media retention analysis

To address the issue of PDMS evaporation, we submerged devices in a shallow dish of deionized water. This method substantially reduced media depletion due to evaporation and PDMS absorption. Even after 24 h, the submerged chips still had approximately 90 % of the GFP solution in the chambers, whereas the non-submerged chips had only 12% of the solution remaining (Fig. 3.5).

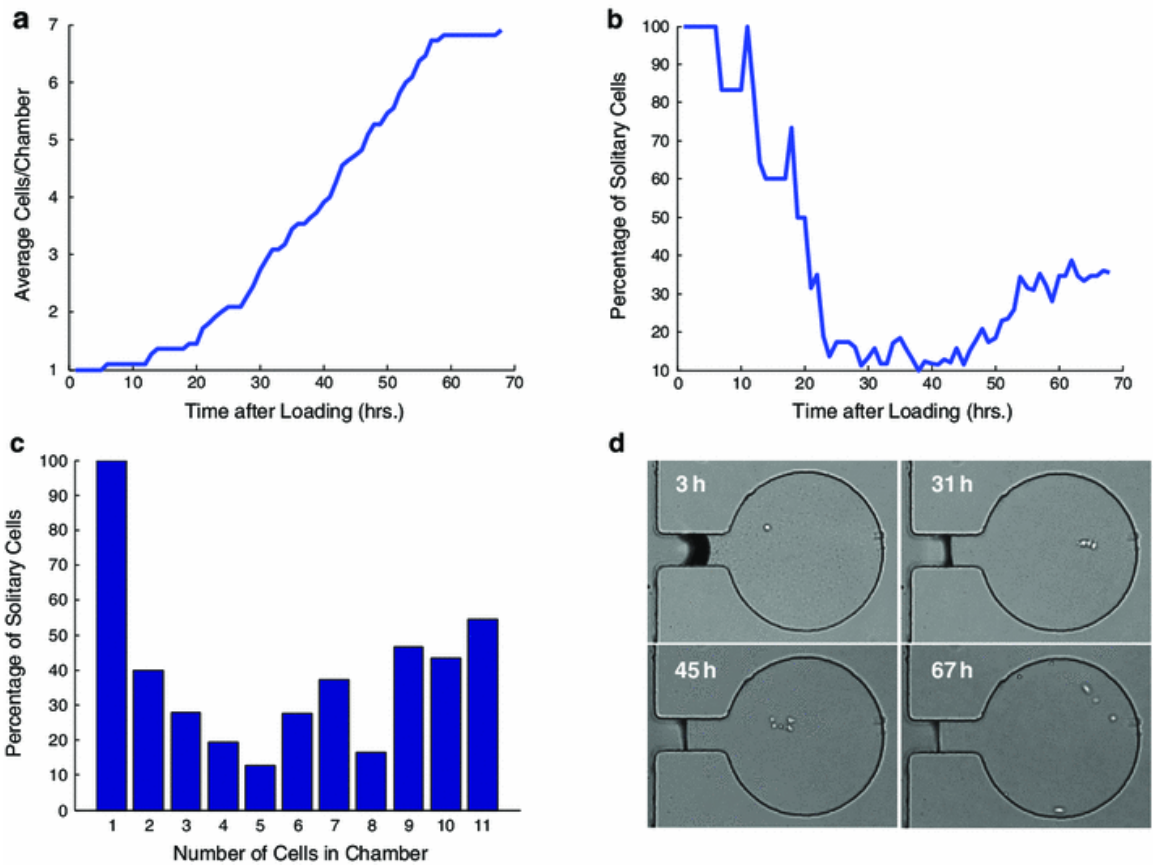

Figure 3.4: Quantitative analysis of choanoflagellates in chambers. a) This graph shows the average number of cells per chamber across 11 selected chambers. b) This graph shows the percentage of solitary cells over time. At the start of the experiment, each chamber had exactly one cell; therefore, all of the cells were in a solitary form. As the average cells/chamber increased, the cells began to form chain colonies, causing the percentage of solitary cells to fall. The percentage of solitary cells increase after 48 h, as cells begin to bud off the colonies. c) This graph illustrates how the percentage of solitary cells vary depending on the number of cells in the chamber. From 1 to 5 cells per chamber, there is a sharp decrease in the number of solitary cells. As the chain colonies grow in size, cells begin to bud off, increasing the percentage of solitary cells. d) Phase-contrast images of one chamber at four time points. At 3 h, a single cell is present in the chamber. The images at 31 and 45 h show that the cell has divided and begun forming a chain colony (with 3 and 5 cells, respectively). After 67 h, the number of cells in the chamber has grown to 7, and the colony has completely disaggregated.

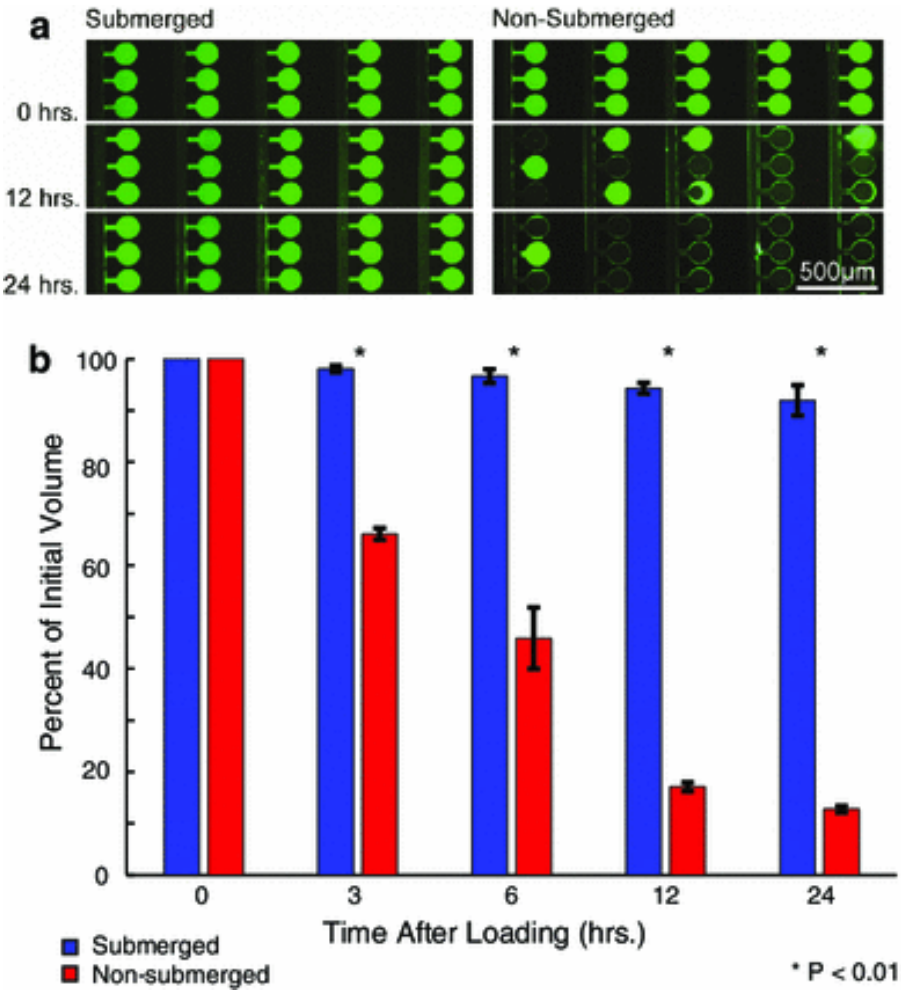

Figure 3.5: Quantitative analysis of media retention. a) Epi-fluorescence photographs taken at 0, 12, and 24 h after evacuation of the serpentine channels demonstrate the effect of submerging the chip on media retention. In the submerged chip, little solution was lost after 24 h; however, the majority of the solution was lost in almost every chamber of the non-submerged chip after 24 h. b) This graph shows the percent of the initial volume of GFP solution in the chambers after 3, 6, 12, and 24 h after loading. All values, obtained by image processing of epi-fluorescence photographs, represent the cross-sectional area of GFP solution retained in the chambers. The blue bars represent the submerged chips, while the red bars represent the non-submerged chips. After 24 h, the non-submerged chips lost approximately 88 % of the solution, nearly 8x more than the submerged chips.

Submerging the devices in water has proven to be an effective and simple means of retaining media in the trapping chambers, enabling long-term experiments. Retention of media is important not only for visualizing cells long term but also for maintaining the concentration of the media components, since solvent evaporation will lead to an increase in solute concentration. For short-term applications where the maintenance of solute concentration is of less concern, submerging might not be necessary. The retention bridge provides time to complete short-term experiments with non-submerged devices. Applying a previously developed algorithm (EPA 1999), we calculated a bridge retention time of 3.65 h, while our experiment showed depletion of bridge media after only 3 h. We attribute the increased rate of media depletion to PDMS absorption of the media (Regehr *et al.* 2009).

Chamber size comparison

We found a positive correlation between chamber size and the rate of proliferation (Fig. 3.6). For the smallest chambers with 30 μm radii, we observed no proliferation, even after 24 h. However, for chambers with 50 and 70 μm radii, after 24 h the number of cells increased by 30% and 50%, respectively.

We propose that the significant effect chamber size has on proliferation can be attributed to nutrient consumption and interactions with the PDMS. Cell growth and division have been shown to be directly related to the cell media's nutrient condition and concentration (Umehara *et al.* 2003). By fluidically isolating

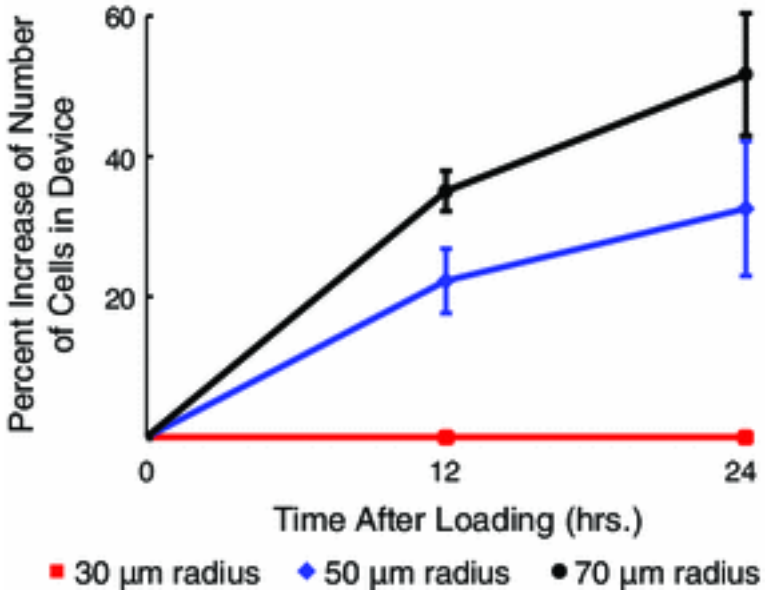

Figure 3.6: Growth dynamics of choanoflagellates in traps. This graph shows the percent increase in number of cells in the device for three different chamber sizes. The largest chambers of 70 µm radius showed the largest percent increase in cells, more than 50 % after 24 h. The 30-µm-radius chambers.

the cells in a given amount of media, we are forming microecosystems with specific ratios of organisms to consumable nutrients. Since most chambers with choanoflagellates contain only one or two cells after loading (regardless of chamber radius), the larger volumes provide more nutrients for these cells and thus increase viability and potential growth rates. Additionally, PDMS oligomers are known to leech into microfluidic devices and adversely affect cell health (Regehr *et al.* 2009). Increasing the chamber size, thereby decreasing its surface-area-to-volume ratio, may reduce this effect.

While the trend would suggest further increasing chamber size to increase cell proliferation, we chose 70 μm as an ideal radius because it allowed visualization of multiple chambers in one field of view while simultaneously yielding adequate proliferation. The specific chamber size needed for a given organism will depend on its specific nutrient consumption rate.

Trapping efficiency analysis

The distribution of cells in the devices varied based on the loaded cell concentration. At very low cell concentrations (100,000 and 500,000 cells/mL), most chambers had no cells, while less than 5% had only one cell. At 2,500,000 cells/mL, over 80% of the chambers were occupied by at least one cell, and nearly a third of the chambers had exactly one cell trapped inside. At the highest concentration of 8,350,000 cells/mL, almost every chamber was filled, but over 85% had two or more cells inside.

We compared the distribution of cells in our device to the Poisson distribution, which assumes that the cells act independently of one another (Fig. 3.7); therefore, the trapping of one cell in a chamber neither increases nor diminishes the chance of another cell being trapped. Although the Poisson model accurately predicts the general trend for the likelihood of a chamber containing 0, 1, or >2 cells, it deviates in certain places, particularly in predicting the percentage of chambers with 1 or >2 cells. This is likely due to the fact that some cells load as clumps.

3.5 Conclusion

Our novel microfluidic platform allows high-throughput visualization of the movement and behavior of motile cells for extended time periods. The device offers a number of advantages over conventional visualization methods, as well as similar microfluidic devices. The conventional method of visualizing cells in a petri dish is low throughput and requires constant tracking to keep the motile cell in the field of view of the microscope. Our easy-to-operate device confines cells to one of many chambers which can be individually observed using an automated stage. Unlike other devices designed for motile organisms, our device traps cells in a hydrostatic environment without immobilizing them, thereby allowing them to move and behave normally.

Our device can be used in a number of different ways. Depending on the study, it could be used either to visualize cells in a few chambers for a long time

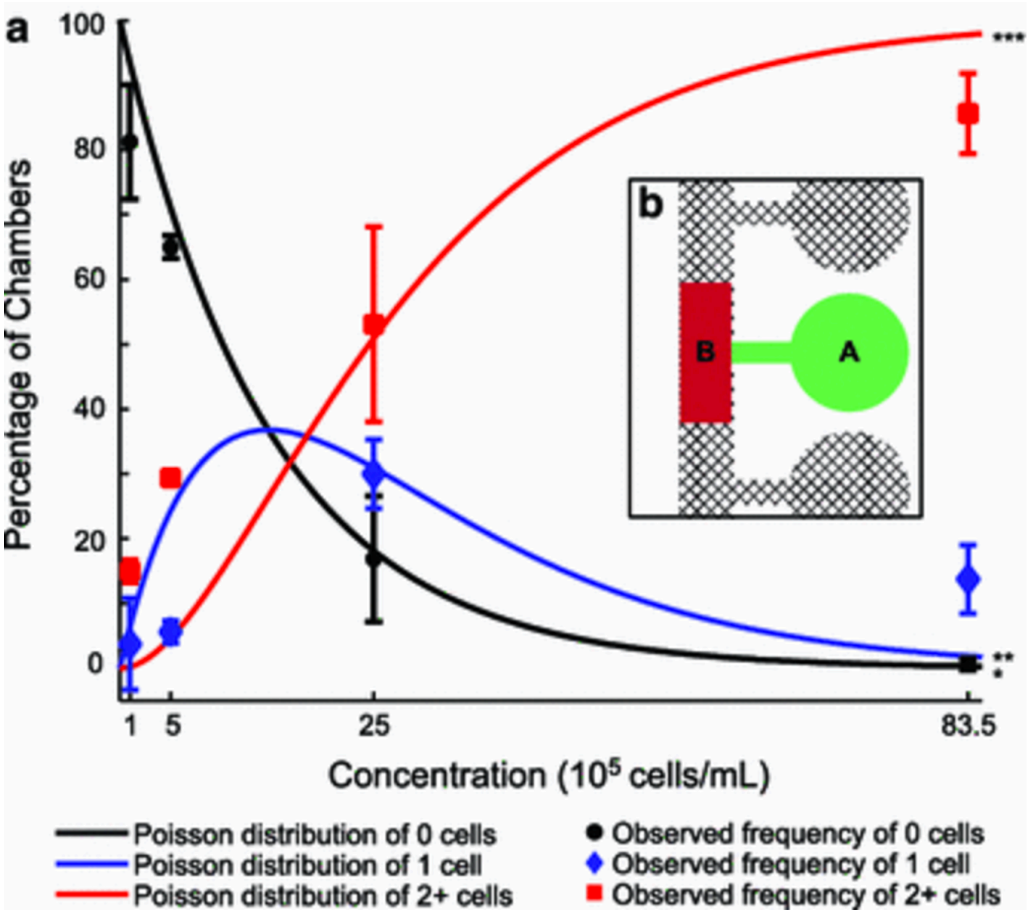

Figure 3.7: Comparison to Poisson distribution. a) The observed frequencies of 0 cells/chamber, 1 cell/chamber, and 2+ cells/chamber are plotted against the expected Poisson distribution for the four different concentrations that we tested. The Poisson distribution provides a reasonable approximation of the distribution of trapped cells in the device. b) The green area (labeled “A”) represents the trapping region, and the red area (labeled “B”) represents the non-trapping region.

period or to image every chamber in the device using an automated stage in order to obtain large sample sizes. The number of chambers, as well as their shapes and sizes, may be tailored to particular experimental needs. We have provided equations for determining the evaporation time of media in the device and the optimal concentration of cells for a desired distribution, which will also aid in experiment design. We anticipate this platform finding many applications in the study of motile cell behavior.

3.6 Acknowledgments

We would like to thank Nicole King, Terry Johnson, Arielle Woznica, and Tera Levin for their mentorship and guidance. We would also like to thank the King laboratory for graciously providing the *S. rosetta* cells. This work was supported by the National Science Foundation's Research Experience for Undergraduates (REU) program under Grant No. 0852058.

Chapter 3 contains material originally published as: Halperin SO, CT Poling CT, Mathrani SR, Turner BW, Greene AC, Dueck ME, Myers F (2014) A massively parallel microfluidic device for long-term visualization of isolated motile cells. Microfluidics and nanofluidics 17(5): 821-829.

3. 7 References

Alegado RA, Brown LW, Cao S, Dermenjian RK, Zuzow R, Fairclough SR, Clardy J, King N (2012) A bacterial sulfonolipid triggers multicellular development in the closest living relatives of animals. eLife.

Balaban NQ (2005) Szilard's dream. Nat Methods 2:648–649.

Breslauer DN, Lee PJ, Lee LP (2006) Microfluidics-based systems biology. Mol BioSyst 2:97–112.

Cira NJ, Ho JY, Dueck ME, Weibel DB (2012) A self-loading microfluidic device for determining the minimum inhibitory concentration of antibiotics. Lab Chip 12:1052–1059.

Di Carlo D, Lee LP (2006) Dynamic single-cell analysis for quantitative biology. Anal Chem 78:7918–7925.

Di Carlo D, Wu LY, Lee LP (2006) Dynamic single cell culture array. Lab Chip 6:1445–1449.

Dimov IK, Basabe-Desmonts L, Garcia-Cordero JL, Ross BM, Ricco AJ, Lee LP (2011) Stand-alone self-powered integrated microfluidic blood analysis system (SIMBAS). Lab Chip 11:845–850.

EPA (1999) Risk management program guidance for offsite consequence analysis. U.S. EPA. EPA-550-B-99-009.

Fairclough SR, Dayel MJ, King N (2010) Multicellular development in a choanoflagellate. Curr Biol 20:R875–R876.

Friedman M, Lindstrom S, Ekerljung L, Andersson-Svahn H, Carlsson J, Brismar H, Gedda L, Frejd FY, Stahl S (2009) Engineering and characterization of a bispecific HER2 × EGFR-binding affibody molecule. Biotech Appl Biochem 54:121–131.

Fu AY, Chou H, Spence C, Arnold FH, Quake SR (2002) An integrated microfabricated cell sorter. Anal Chem 74:2451–2457.

Groisman A, Lobo C, Cho H, Campbell JK, Dufour YS, Stevens AM, Levchenko A (2005) A microfluidic chemostat for experiments with bacterial and yeast cells. Nat Methods 2:685–689.

Ingham CJ, Vlieg JETVH (2008) MEMS and the microbe. Lab Chip 8:1604–1616.

Kim SM, Lee SH, Suh KY (2008) Cell research with physically modified microfluidic channels: a review. Lab Chip 8:1015–1023.

King N (2004) The unicellular ancestry of animal development. Dev Cell 7:313–325.

King N (2005) Choanoflagellates. Curr Biol 15:R113–R114.

Kumano I, Hosoda K, Suzuki H, Hirata K, Yomo T (2012) Hydrodynamic trapping of *Tetrahymena thermophila* for the long-term monitoring of cell behaviors. Lab Chip 12:3451–3457.

Lang BF, O'Kelly C, Nerad T, Gray MW, Burger G (2002) The closest unicellular relatives of animals. Curr Biol 12:1773–1778.

Lindstrom S, Andersson-Svahn H (2010) Overview of single-cell analyses: microdevices and applications. Lab Chip 10:3363–3372.

Lindstrom S, Andersson-Svahn H (2011) Miniaturization of biological assays—overview on microwell devices for single-cell analyses. Biochim Biophys Acta 1810:308–316.

Lindstrom S, Eriksson M, Vazin T, Sandberg J, Lundeberg J, Frisen J, Andersson-Svahn H (2009a) High-density microwell chip for culture and analysis of stem cells. PLoS ONE 4:e6997.

Lindstrom S, Hammond M, Brismar H, Andersson-Svahn H, Ahmadian A (2009b) PCR amplification and genetic analysis in a microwell cell culturing chip. Lab Chip 9:3465–3471.

Liu W, Dechev N, Foulds IG, Burke R, Parameswaran A, Park EJ (2009) A novel permalloy based magnetic single cell micro array. Lab Chip 9:2381–2390.

Luo C, Zhu X, Yu T, Luo X, Ouyang Q, Ji H, Chen Y (2008) A fast cell loading and high throughput microfluidic system for long-term cell culture in zero flow environments. Biotechnol Bioeng 101(1):190–195.

Lutz BR, Chen J, Schwartz DT (2006) Hydrodynamic tweezers: 1. Noncontact trapping of single cells using steady streaming microeddies. Anal Chem 78:5429–5435.

Mao H, Cremer PS, Manson MD (2003) A sensitive, versatile microfluidic assay for bacterial chemotaxis. Proc Natl Acad Sci 100:5449–5454.

Muralimohan A, Eun YJ, Bhattacharyya B, Weibel DB (2009) Dissecting microbiological systems using materials science. Trends Microbiol 17:100–108.

Nilsson J, Evander M, Hammarstrom B, Laurell T (2009) Review of cell and particle trapping in microfluidic systems. Anal Chim Acta 649:141–157.

Novick A, Szilard L (1950) Description of the chemostat. Science 112:715–716

Regehr KJ, Domenech M, Koepsel JT, Carver KC, Ellison-Zelski SJ, Murphy WL, Schuler LA, Alarid ET, Beebe DJ (2009) Biological implications of polydimethylsiloxane-based microfluidic cell culture. Lab Chip 9:2132–2139.

Umehara S, Wakamoto Y, Inoue I, Yasuda K (2003) On-chip single-cell microcultivation assay for monitoring environmental effects on isolated cells. Biochem Biophys Res Commun 305:534–540.

Wain AR (2011) Patterns of growth and culturing protocols for *Salpingoeca rosetta* to be used in investigations of the origin of animal multicellularity. University of Akron (Master's thesis)

Weibel DB, Diluzio WR, Whitesides GM (2007) Microfabrication meets microbiology. Nat Rev Microbiol 5:209–218.

Xia Y, Rogers JA, Paul KE, Whitesides GM (1999) Unconventional methods for fabricating and patterning nanostructures. Chem Rev Columb 99:1823–1848.

Zheng S, Lin H, Liu J, Balic M, Datar R, Cote RJ, Tai Y (2007) Membrane microfilter device for selective capture, electrolysis and genomic analysis of human circulating tumor cells. J Chromatogr A 1162:154–161.

Chapter 4: A self-loading microfluidic device for determining the minimum inhibitory concentration of antibiotics

4.1 Abstract

This article describes a portable microfluidic technology for determining the minimum inhibitory concentration (MIC) of antibiotics against bacteria. The microfluidic platform consists of a set of chambers molded in poly(dimethylsiloxane) (PDMS) that are preloaded with antibiotic, dried, and reversibly sealed to a second layer of PDMS containing channels that connect the chambers. The assembled device is degassed via vacuum prior to its use, and the absorption of gas by PDMS provides the mechanism for actuating and metering the flow of fluid in the microfluidic channels and chambers. During the operation of the device, degas driven flow introduces a suspension of bacterial cells, dissolves the antibiotic, and isolates cells in individual chambers without cross contamination. The growth of bacteria in the chambers in the presence of a pH indicator produces a colorimetric change that can be detected visually using ambient light. Using this device we measured the MIC of vancomycin, tetracycline, and kanamycin against *Enterococcus faecalis* 1131, *Proteus mirabilis* HI4320, *Klebsiella pneumoniae*, and *Escherichia coli* MG1655 and report values that are comparable to standard liquid broth dilution measurements. The device provides a simple method for MIC determination of individual antibiotics against human pathogens that will have applications for clinical and point-of-care medicine. Importantly, this device is designed around

simplicity: it requires a single pipetting step to introduce the sample, no additional components or external equipment for its operation, and provides a straightforward visual measurement of cell growth. As the device introduces a novel approach for filling and isolating dead-end microfluidic chambers that does not require valves and actuators, this technology should find applications in other portable assays and devices.

4.2 Introduction

In this study we describe the characterization and implementation of a self-loading microfluidic device for determining the minimum inhibitory concentration (MIC) of antibiotics against several bacterial strains, including human pathogens. The MIC of a compound is defined as the lowest dose that inhibits the growth of a microbe in a set time interval, and the determination of this value is an important clinical step in the prescription of effective antibiotics. As the resistance of bacteria to drugs continues to increase and the discovery rate of new antibiotics declines, this assay will continue to grow in importance for positive patient outcomes and for preventing the prescription of ineffective antibiotics that increase the spread of resistance (Neu 1992, Levy 2004).

MIC assays are traditionally performed using diffusion or dilution methods. In diffusion methods, a hydrophilic strip or disc is infused with antibiotic and placed in contact with the surface of an agar plate upon which a microbe is growing. The antibiotic diffuses radially through the agar gel and forms a

concentration gradient that inhibits microbial growth close to the strip or disc. The formation of a visual ‘zone of inhibition’ in this assay enables the MIC to be estimated. Diffusion-based assays are technically simple to perform, however they have several disadvantages. For example, the results of the assays must be standardized to the specific characteristics of the agar growth media, which strongly influence diffusion of the antibiotics. Additionally, the analysis of these assays is subjective and variable (Ge 2002).

In dilution methods, microbes are inoculated in a series of separate culture tubes or onto separate agar plates containing nutrient media and a two-fold serial dilution of an antimicrobial agent. Guidelines for dilution-based methods of determining MIC values are published in the US by the Clinical Laboratory and Standards Institute (CLSI) and by institutions in other countries. The MIC is determined by identifying the lowest concentration of antibiotic that inhibits microbial growth, and is typically measured by visual inspection. These assays are well characterized and provide a more quantitative readout than diffusion methods, however they are generally more labor intensive. The use of a liquid handling robot to prepare dilution series in multiwell plates can reduce the time and labor involved, however these instruments are expensive and not widely available in labs.

Microfluidic technologies provide a platform for combining the simplicity of diffusion methods with the quantitative results of dilution methods. Several

microfluidic devices that perform MIC assays have been reported. These devices have focused on reducing the assay time or increasing assay throughput by utilizing high aspect ratio channels (Chen 2010), plugs of fluid (Beodicker 2008), microparticles (Eun 2011), concentration gradient generators (Kim 2010), and dielectrophoresis (Peitz 2010). As these designs represent a significant departure from standard CLSI methodology, they require characterization with a panel of bacterial strains and antibiotics before they can be implemented as clinical devices.

Previously described designs require multiple technical steps and additional equipment for use. For example, a common requirement is that users create a concentration gradient off-chip and introduce the liquid into the device using a syringe pump. The multiple steps involved in gradient formation increase technician training, assay setup time, and user error. Requiring additional external equipment—such as a syringe pump—increases the cost and technical expertise needed to operate devices. These characteristics are potential barriers for the adoption of devices in clinics and as point-of-care diagnostics (Chin 2007, Yager 2006). The introduction of a simple device technology that requires no additional external equipment for its operation would reduce cost, user error, and the training of technicians, and may provide a universal assay for use in a range of different environmental contexts. A microfluidic platform that combines these characteristics to measure the MICs of different antibiotics against different bacteria has not yet been described.

This study describes an autonomous microfluidic device that measures the MIC of antibiotics against different species of bacteria. Importantly, this device is designed around simplicity: it requires a single user pipetting step to introduce the sample, no additional components or external equipment for its operation, and provides a straightforward visual measurement of cell growth. The technology introduces a new solution for filling and isolating dead-end microfluidic chambers that does not require valves and actuators. The device consists of a set of chambers molded in poly(dimethylsiloxane) (PDMS) that are preloaded with antibiotic, dried, and reversibly sealed to a second layer of PDMS containing channels that connect the chambers (Fig. 1). The assembled device is degassed via vacuum prior to its use, and the absorption of gas by PDMS provides the mechanism for actuating and metering the flow of fluid in the microfluidic channels and chambers (Hosokawa 2004, Dimov 2011). After loading and assembly devices can be vacuum sealed for distribution and use. The end user only needs to open the packaging and pipette a drop of sample on the inlet port. Degas driven flow—created by the degassed PDMS layers—then introduces the suspension of bacterial cells, dissolves the antibiotic, and isolates cells in individual chambers without cross contamination. The growth of bacteria in the chambers in the presence of a pH indicator produces a colorimetric change that can be detected visually using ambient light without a microscope. Using this device we measured the MICs of vancomycin, tetracycline, and kanamycin against *Enterococcus faecalis* 1131, *Proteus mirabilis* HI4320, *Klebsiella*

pneumoniae, and *Escherichia coli* MG1655 and report values that are comparable to standard liquid broth dilution measurements. The device provides a simple method for MIC determination of individual antibiotics and combinations of antibiotics against human pathogens that will have clinical applications.

4.3 Methods

Fabrication of microfluidic devices

Devices were fabricated using soft lithography (Duffy 1998). Briefly, we fabricated masters in SU-8 photoresist (Microchem) on silicon wafers using photolithography. We created separate masters for the chamber and channel sections of the device. Each chamber was 300-μm tall and 2-mm wide and had a volume of 0.98 μL, including the side-channel that connected it to the main channel. The channel height was 50 μm and the width ranged from 150–260 μm. PDMS (Sylgard 184: Dow Corning) was mixed in a 1:10 ratio (base:cross linking agent), cast against the master to a height of ~1 mm, and cured at 65 °C overnight. The layer of PDMS containing the chambers was peeled away from the master and trimmed with a razor. Before use, ten different concentrations of antibiotic were pipetted (2.94 μL, Fig. 4.1a) into the 10 separate chambers and dried. The volume of liquid exceeded the volume of the chamber, however surface tension kept each droplet pinned within a chamber ensuring that all dissolved antibiotic was deposited within the chamber upon drying. The channel layer was peeled away from the mold and trimmed with a razor. A 3 mm diameter vacuum hole and a 1 mm diameter inlet port were punched in the channel

section using tissue culture bores (Harris UniCore, Tedpella) (Fig. 4.1b). The two PDMS layers (chambers and channels) were aligned and assembled by reversibly bonding the feature sides together creating ten culture chambers that were connected by channels. A plastic slip was placed on top of the channel section to convert the vacuum hole into a chamber; the sole inlet port remained uncovered (Fig. 4.1c). The device was placed in a vacuum for 30 min at ~25 kPa (Fig. 4.1d). To test whether these devices could be packaged under vacuum for later use, we incubated devices in a vacuum (~25 kPa), removed them, and immediately sealed them in plastic FoodSaver food storage bags using a household kitchen grade vacuum sealer (FoodSaver V3835). We tested the loading of these devices up to 83 days later.

Off-chip MIC measurements

To validate our experimental data with the microfluidic device, we performed off-chip MIC assays using the broth dilution method according to CLSI protocols. Briefly, we prepared antibiotic stock solutions (10 mg mL^{-1}) of vancomycin hydrochloride (MP Biomedicals), tetracycline hydrochloride (Eastman Kodak), and kanamycin monosulfate (Fisher BioReagents) in sterile deionized water. We made a 1:10 dilution series of the stock solutions in cation-adjusted Mueller-Hinton broth (CAMHB). Appropriate volumes of these dilutions were added to CAMBH (pH 7.3) to create a two-fold series dilution in which the total volume was 1 mL. We prepared cell solutions of *E. faecalis* (1131), *P. mirabilis* (HI4320), *K. pneumoniae*, and *E. coli* (MG1655) in 13 × 100 mm tubes

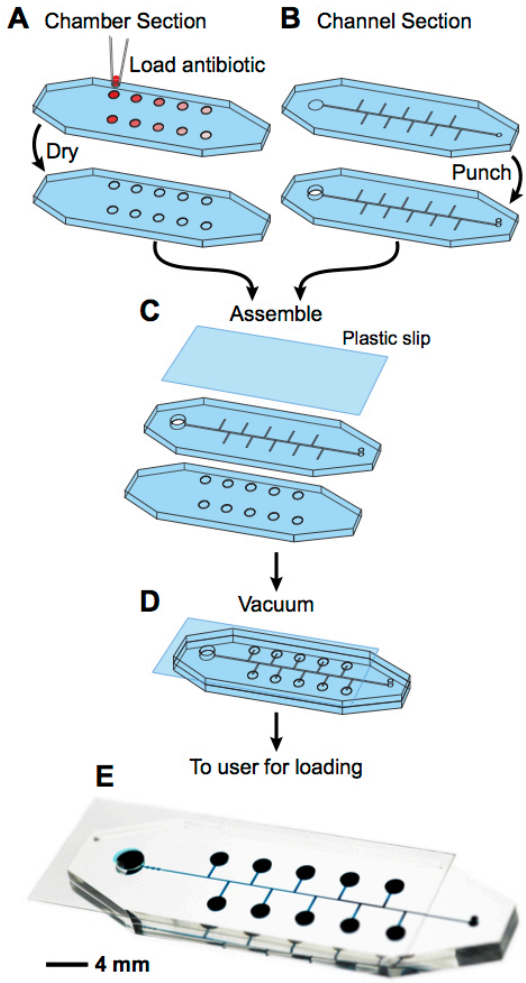

Figure 4.1: Schematic of device assembly. (A) Chambers embossed in a layer of PDMS are loaded with solutions of antibiotic at different concentrations and the liquid is evaporated. (B) In a separate layer of PDMS, holes are punched at the ends of the center channel to form an inlet port and a larger vacuum chamber. (C) The device is assembled by aligning the microfluidic channels in one layer of PDMS with the chambers in the second layer of PDMS; microfluidic channels now connect the chambers. A plastic slip is placed over the vacuum chamber to seal it. (D) The device is incubated in a vacuum, removed, and is ready for sample loading by the user. (E) An image of an assembled device in which the channels and chambers are filled with a blue dye to make them visible.

by adjusting the concentration of cells in overnight cultures to match the turbidity of a 0.5 McFarland standard (~10^8 CFU/mL) using CAMHB. We diluted the solutions 100-fold in CAMHB and added 1 mL of the suspension to 1 mL of antibiotic solution—prepared as described above—to yield a final cell concentration of ~5 × 10^5CFU/mL. We incubated the cultures for 20 h in a humidified incubator at 35 °C (no shaking) with the exception of experiments with vancomycin and *E. faecalis*, which was incubated for 24 h according to CLSI protocols. We determined the MIC as the lowest concentration of antibiotic at which no growth was visible after incubation.

On-chip MIC measurements

To perform on-chip MIC measurements, we used procedures that mimicked the CLSI guidelines with minor adjustments. We prepared antibiotic stock solutions (10 mg mL^{-1}) of vancomycin hydrochloride, tetracycline hydrochloride, and kanamycin monosulfate in sterile deionized water. We made a 1:10 dilution series of the stock solutions in sterile deionized water. Appropriate amounts of these dilutions were added to sterile deionized water to create a two-fold dilution series in which the final antibiotic concentration in the chambers ranged from 0.5–1024 μg mL^{-1}. To avoid the error associated with pipetting ~1 μL of liquid to each chamber, we diluted each antibiotic stock solution 3x and pipetted 2.94 μL (3× volume) to each chamber. We placed the layer of the PDMS containing the chambers in a laminar flow hood to evaporate the liquid then assembled the devices and placed them under vacuum. Cell suspensions were

prepared by adjusting the concentration of cells in overnight cultures to match the turbidity of a 0.5 McFarland standard (~10^8 CFU/mL) using CAMHB media, pH 7.3. We diluted the standardized culture 1:200 in CAMBH media, pH 8.2 supplemented with 1% glucose and 0.05% phenol red to provide a colorimetric change upon growth. We removed the devices from the vacuum and placed 20 µL of cell suspension on the inlet port. The antibiotic was dissolved by the cell suspension in each chamber to yield the desired final concentration. To be consistent with the CLSI guidelines, we incubated devices for 18 h at 35 °C in a humidified incubator. We determined the MIC as the lowest concentration of antibiotic in which bacteria did not grow. Bacterial growth changed the pH of the liquid nutrient media containing the indicator phenol red, and produced a visible color change that we used to identify the cell growth in chambers and ultimately the MIC for that particular strain.

Isolating resistant mutants to kanamycin

We created kanamycin resistant mutants from wild type bacteria to determine whether the microfluidic device could detect their increased resistance to the antibiotic. We plated 100 µL of an overnight culture of E. coli MG1655 on LB agar plates supplemented with 16 µg mL^{-1} kanamycin; the antibiotic concentration was ~2× the MIC of kanamycin that we measured against *E. coli* MG1655. After overnight incubation at 35 °C we identified 24 colonies that grew in the presence of 16 µg mL^{-1} kanamycin. We picked one of these colonies and characterized its sensitivity to kanamycin in the microfluidic device.

Determining chamber to chamber cell distribution

We determined the distribution of cells loaded into the chambers of six separate devices (n = 60 chambers) using an *E. coli* MG1655 strain constitutively expressing enhanced green fluorescence protein off a plasmid. We grew cells overnight at 30 °C in shaking incubator (New Brunswick Scientific) at 200 rpm. The cells were grown in LB media containing 100 μg mL^{-1} ampicillin and 1mM IPTG for resistance selection and fluorescence induction, respectively. We diluted the culture of cells to the 0.5 McFarland standard using fresh LB and the standardized solution was further diluted 1:200 in PBS. We loaded cells into the chambers of the device as described for the on-chip MIC experiments. Once the devices were loaded, we imaged the fluorescence intensity of each chamber using a 4× objective on an inverted microscope (Nikon Eclipse TE2000) and analyzed the images using ImageJ. We transformed each image into an 8-bit binary image using the max entropy threshold (Sahoo 1998) with a dark background to prepare it for particle analysis and to remove background noise. Once the images were transformed, we used the ImageJ Analyze Particles function with size limited to 0–15 $pixels^2$ and circularity of 0.080–1.00 to identify the number of fluorescent cells per chamber.

4.4 Results and Discussion

Device Specifications

The MIC devices consisted of a single, center channel (50-μm tall, 150-μm wide) that connected a circular inlet port (1 mm diameter, ~1 mm tall, ~1.6 μL

volume) on one end and a circular vacuum chamber (3 mm diameter, ~1 mm tall, ~7.1 μL volume) located at the other end (Fig. 1). Along the length of the center channel, we positioned 10 circular culture chambers (2 mm diameter, 300 μm tall, 0.98 μL volume). Each culture chamber was connected to the center channel by a single straight channel (3.2 mm long, 260 μm wide, 50 μm tall). We fabricated the devices in PDMS to take advantage of the permeability of the polymer (for actuation of the fluid) and the rapid prototyping capabilities of PDMS microfluidic devices (Duffy 1998, Xia 1998).

Loading the device

We designed portable MIC devices with several features to eliminate user steps and external equipment. First, the device contains a self-loading mechanism that uses degas driven flow to draw a sample into the microfluidic channels and chambers (Hosokawa 2004). The operation of the device consisted of two steps: (1) removal from a vacuum and (2) introduction of a droplet of sample (20 μL) at the inlet port. Dissolved gas in the PDMS layers was removed during vacuum degasing according to Henry's law, $c = kP$ where c is the molar concentration of dissolved gas (in M), P is the pressure of gas over the liquid (in atm; we consider PDMS to be a viscous liquid), and k is a temperature-dependent constant (in M atm). When removed from vacuum, degassed PDMS absorbs gas from the environment, which creates a vacuum within the channels and chambers, and produces degas driven flow of the fluid located at the inlet port. To demonstrate the loading of devices, we introduced a different

concentration of blue dye to all ten chambers, evaporated the liquid, assembled a microfluidic device, and vacuum degased the PDMS. We removed the device from the vacuum, placed a 20 μL droplet of a solution of yellow dye on the inlet, and imaged the process (Fig. 4.2).

Second, the microfluidic system was designed to partition the sample into discrete chambers containing reagents and to isolate each chamber from the rest of the device. As degas driven flow fills the device with fluid, the air in the chambers is pulled out through the PDMS, and the dried antibiotics in the culture chambers are dissolved. We designed the culture chambers such that their individual volumes (0.98 μL) were much smaller than the volume of the vacuum chamber (~7.1 μL), and thus the fluid entering the channel through the inlet port filled the culture chambers before the vacuum chamber (Fig. 4.2a). After the culture chambers were filled, degas driven flow continued to pull fluid into the vacuum chamber until the liquid sample in the inlet port was consumed. Air was then pulled into and through the center channel to the vacuum port, isolating the fluid in each culture chamber. Layering a droplet of oil on top of the liquid sample made it possible to introduce an insulating layer of oil—instead of air—that isolated the sample in the chambers (data not shown). Using degas driven flow prevents the requirement of valves or other actuators and external equipment to load the device and isolate the chambers.

Flows through the center channel and side channels of the device were

unidirectional and prevented the contents of the culture chambers from mixing and becoming contaminated (Fig. 4.2b). Using the loading protocol we adopted (described in the Materials and Methods section), we observed a period of time (~18 min) after fluid filled the culture chambers during which the reagents could diffuse out of the chambers into the central channel. We designed relatively long side channels (3.2 mm long) that connected the culture chambers to the center channel to prevent diffusion of antibiotic into other chambers before the liquid in the culture chambers was isolated (Fig. 4.2c). To minimize the impact of any diffusion that occurred, we filled the culture chambers located closest to the vacuum chamber with the highest concentration of antibiotics; the concentration of antibiotics decreased in chambers located close to the inlet port. As flow in the center channel of the device is constant and unidirectional from the inlet to the vacuum chamber, this configuration of antibiotics ensures that any diffusion would be from low concentrations of antibiotic into higher antibiotic concentrations and would thus have a minimal impact on the assay.

Reproducibility of device loading

To characterize the reproducibility of controlling the concentration of reagents in the chambers, we fabricated five devices and loaded each of the chambers with a different concentration of fluorescein (18–99 μM) with a pipette. We dried the solutions, assembled and vacuum degassed the PDMS devices, and introduced a 20 μL droplet of deionized water at the inlet. After the liquid was introduced and isolated in the chambers, we imaged the fluorescence intensity of

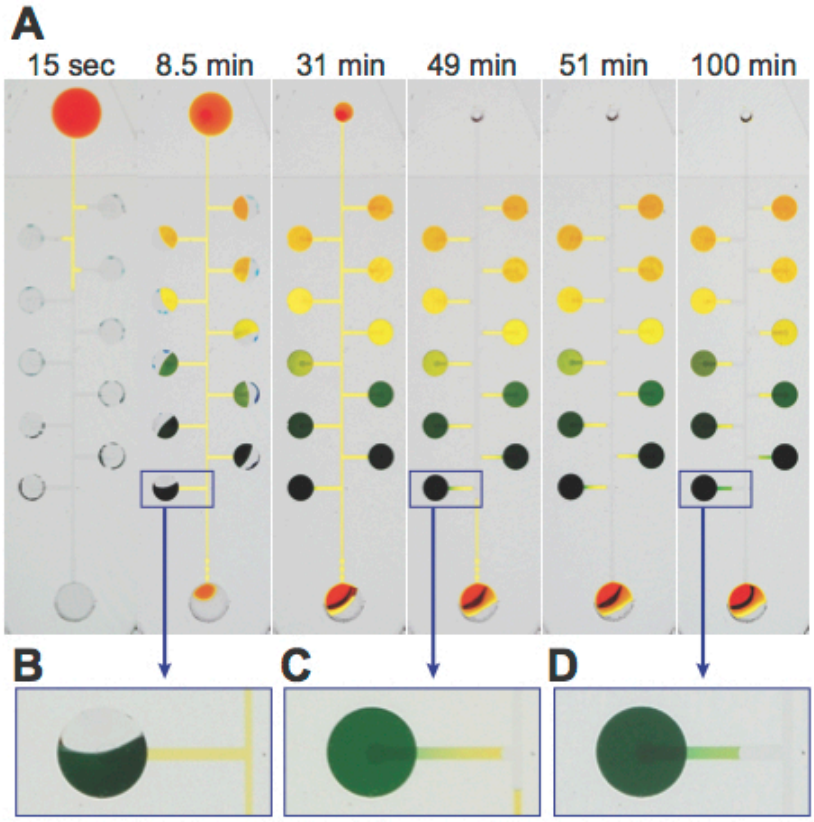

Figure 4.2: Time course of device loading. Chambers were loaded with different concentrations of blue dye with a pipette. After evaporating the liquid, the devices were assembled and vacuum degassed. (A) A sequence of images that illustrates the loading of a 20 μL droplet of yellow dye placed at the inlet port of the freshly degassed PDMS device. The liquid immediately filled the central channel and then filled the culture chambers. The vacuum chamber continued to draw in the fluid until the droplet was consumed, at which point air was pulled into the device and traveled down the central channel isolating the fluid in the individual culture chambers. The box indicates the region of the culture chamber depicted in B–D. (B) An image of a culture chamber demonstrating that the flow of liquid was unidirectional and prevented the outward diffusion of the content of the chamber. (C) After each chamber was filled with fluid, the chamber was isolated with air before an appreciable amount of dye diffused out of the chamber. (D) An image demonstrating fluid isolation, diffusion within the chamber created a uniform dye distribution

the chambers, and quantified fluorescence intensity using ImageJ (Fig. 4.3b). The mean fluorescence intensity of each chamber (n = 5) between the five devices followed a linear trend.

To determine the distribution of cells from chamber to chamber, we prepared and loaded our devices (60 chambers) with *E. coli MG1655* cells that constitutively expressed enhanced green fluorescent protein. We imaged the fluorescence intensity of each chamber and determined the number of cells using ImageJ. The mean number of cells per chamber was 36 ± 12 cells. We found no significant correlation between chamber position and cells/chamber (failure to reject slope = 0 for cells/chamber vs. chamber position, p = 0.50). Assuming a uniform distribution of cells suspended in culture media at a density of 5×10^5cells mL^{-1}, we expected that each chamber and its connecting side-channel would contain ~500 cells. Our average cell counts are an order of magnitude lower than expected because our inability to capture the entire chamber in one focal plane prevented us from imaging all of the cells. An optical system designed specifically for this platform would solve this deficiency.

Comparing the growth of antibiotic resistant and susceptible strains

To determine whether we could discriminate between antibiotic resistant and susceptible strains of bacteria using the device, we isolated an *E. coli* MG1655 mutant that was resistant to kanamycin and compared it to the wild type parent strain. We loaded the chambers of two devices with a range of

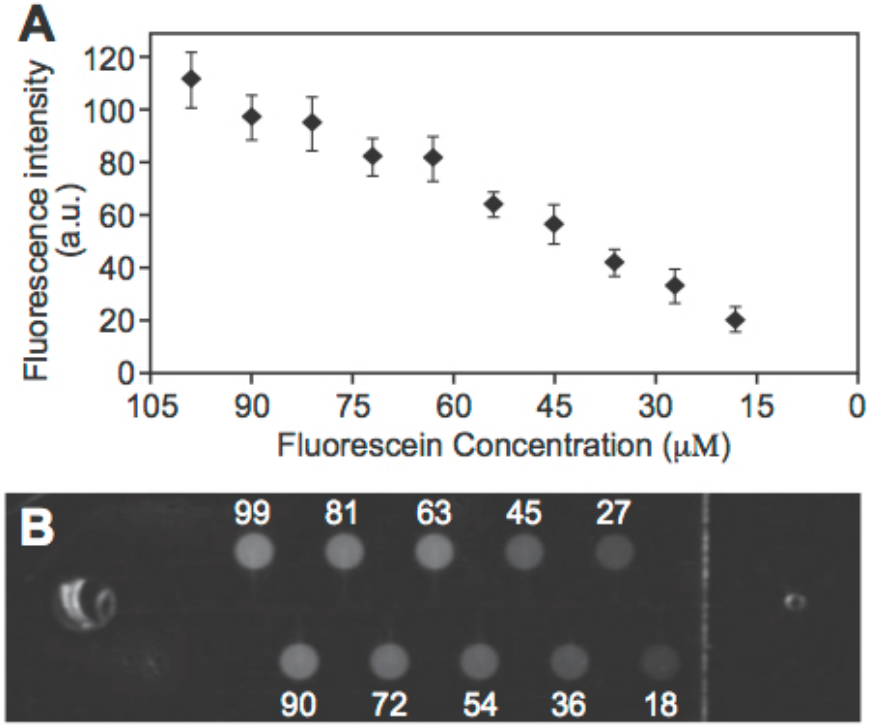

Figure 4.3: Reproducibility of reagent loading. Demonstration of the reproducibility of loading reagents in the chambers. The chambers of a device were loaded with different concentrations of fluorescein (18–99 μM) and the fluid was evaporated. A 20 μL droplet of water was introduced at the inlet, filled the chambers, and isolated the fluid via degas driven flow. (A) A plot depicting average fluorescence intensity of each chamber. Error bars represent the standard deviation of the mean calculated from the chambers of five devices. (B) An image of the fluorescence intensity from each chamber. The concentration of fluorescein (μM) is indicated adjacent to each chamber.

concentrations of kanamycin (final concentration 2–1024 μg mL^{-1}), evaporated the liquid, assembled the devices, and placed them under vacuum. After removing the devices from the vacuum we introduced an aliquot (20 μL) of a suspension of cells of the resistant strain on the inlet of one device and an aliquot (20 μL) of a suspension of cells of the wild type strain on the second device; de-gas driven flow filled and isolated the samples in the chambers. We incubated the devices for 18 h at 35°C in a humidified incubator.

To eliminate external equipment needed for interpreting the test results, we incorporated a pH sensor to indicate cell growth. We added the pH indicator phenol red (0.05% w/v) and glucose (1% w/v) to CAMHB media and adjusted the pH to 8.2. We chose phenol red as it produces a distinct color change close to neutral pH and is not absorbed by PDMS. At the initial pH of the nutrient media, 8.2, phenol red appears bright red. The metabolism of glucose (or other sugars) by bacteria produces organic acids and decreases the pH of nutrient media. The pH change in the chambers of our device (pH < 6.8) made the phenol red in the nutrient media appear bright yellow. Importantly, the change in color was only observed in chambers in which bacteria grew. We were thus able to determine the MIC of the kanamycin resistant *E. coli* strain and the susceptible strain by visually identifying the chamber containing the lowest concentration of kanamycin in which the pH indicator remained red. We determined the MIC of the resistant strain to be 64 μg mL^{-1} and the wild type strain to be 4 μg mL^{-1} (Fig. 4.4). To verify the results from the microfluidic devices, we performed standard liquid

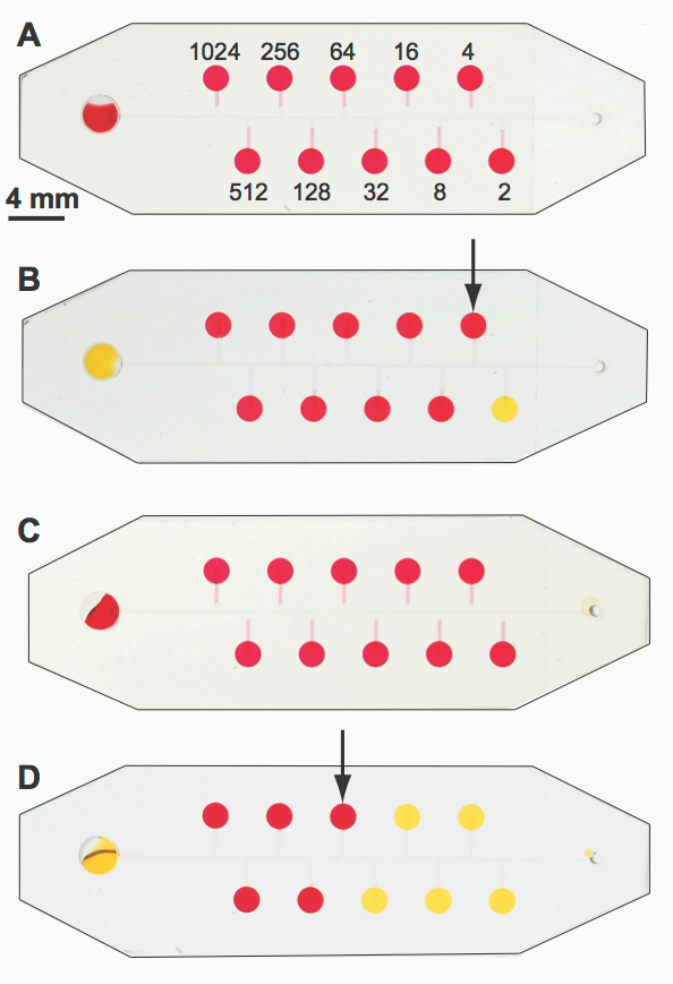

Figure 4.4: Differentiating antibiotic resistance phenotypes. Images depicting the measurement of MIC values of wild type *E. coli* MG1655 and a kanamycin resistant strain of *E. coli* MG1655 in two parallel microfluidic devices. In both devices the concentration of kanamycin ranged from 1024 μg mL^{-1} to 2 μg mL^{-1} (from left to right). Yellow chambers indicate bacterial cell growth. (A–B) Images of *E. coli* MG1655 after 0 h (A) and at 18 h (B) of incubation. The MIC was determined to be 4 μg mL^{-1}, is indicated by the arrow, and represents the lowest concentration at which there was no growth and the chamber appeared red. (C–D) Images of the kanamycin resistant *E. coli* MG1655 strain after 0 h (C) and 18 h (D). The MIC for the resistant strain was 64 μg mL^{-1} and is indicated by the arrow. The concentration of antibiotic (μg mL^{-1}) is indicated adjacent to each chamber. A black line was drawn around the edge of each device to aid in visualization.

broth dilution assays as described in the materials and methods section. Using the dilution technique, we measured the MIC of the resistant strain to be 128 μg mL^{-1} and the wild type strain to be 8 μg mL^{-1}. For both the resistant and the wild type organisms the standard assay results agreed within ±1 two-fold dilution (an acceptable discrepancy according to the CLSI).

Comparing on-chip and off-chip MIC measurements

We validated on-chip MIC measurements against off-chip, broth dilution techniques using: *E. faecalis* (1131), *P. mirabilis* (HI4320), *K. pneumoniae*, and *E. coli* (MG1655), and the antibiotics: vancomycin, tetracycline, and kanamycin. We chose these bacterial species to include Gram-positive (*E. faecalis*) and Gram-negative (*E. coli, P. mirabilis, and K. pneumoniae*) organisms from four different clinically relevant families. We chose three different classes of antibiotics that inhibit different targets and have activity against Gram-negative and Gram-positive bacteria. Vancomycin inhibits the maturation of the peptidoglycan layer of the cell wall during growth, and is specific for treating Gram-positive bacteria. Tetracycline is a broad-spectrum antibiotic that inhibits protein synthesis via binding to the 30S subunit of the ribosome. Kanamycin is a relatively broad-spectrum antibiotic that binds the 30S subunit of the ribosome and causes the mistranslation of proteins.

We observed that bacteria growing in devices reached their MIC values faster than in off-chip assays. Others researchers have noticed this effect and

hypothesized that rapid gas exchange due to the high surface area to volume ratio of micron-scale features combined with the gas permeability of PDMS may be responsible for the reduced response time (Chen 2010). In the interest of replicating the assay conditions and results from the standard CLSI clinical assay, we performed on-chip MIC measurements at the beginning of the suggested time period for most bacterial species (18 h) and off-chip measurements at the end of the suggested time period (20 h). The only exception was the measurement of the MIC of vancomycin against *E faecalis* for which the recommendation is 24 h, however in our experiments we did not observe any change from the 20 h MIC reading. Although these devices provide an opportunity to explore the lower time limit for detecting and measuring antibiotic sensitivity of resistant organisms, such assays would require the definition of a new metric that differs from the clinically defined MIC. We found that the results of our MIC measurements on-chip closely matched those performed-off chip (Table 4.1). The on-chip measurements were all within a two-fold dilution of the MIC values determined off-chip, which is an acceptable discrepancy when comparing assay results according to the CLSI value.

Evaluating bacterial susceptibility to multiple antibiotics

In clinical microbiology, a strain is classified as susceptible, intermediate, or resistant based on the relationship of the MIC of an antibiotic to specified ‘breakpoint’ values (Williams 1990). The breakpoint values are set by organizations, such as the CLSI, and take into consideration MIC values of wild

Table 4.1: Comparing on-chip and off-chip MIC measurements. MIC measurement for a panel of antibiotics against bacteria on- and off-chip. shows the MIC results (μg mL^{-1}) from the device and from the conventional off-chip broth dilution method of MIC determination for vancomycin, tetracycline, and kanamycin against *E. faecalis*, *P. mirabilis*, *K. pneumoniae*, and *E. coli*. In all cases the results match the off chip data within one, two-fold dilution.

	Vancomycin		Tetracycline		Kanamycin	
Species	**On-chip**	**Off-chip**	**On-chip**	**Off-chip**	**On-chip**	**Off-chip**
Enterococcus faecalis	8	4	64	32	128	64
Proteus mirabilis	>1024	>1024	128	256	8	4
Klebsiella pneumoniae	>1024	>1024	8	8	2	2
Escherichia coli	512	256	2	1	4	8

type strains, pharmacokinetic/pharmacodynamic data, and clinical outcomes. Breakpoint values are available for specific clinically relevant pairings of bacterial species and antibiotics and enable clinical decisions without knowing the exact MIC value.

We utilized our microfluidic device to simultaneously test the susceptibility of a microorganism to multiple antibiotics using breakpoint values. To test the antibiotic susceptibility using breakpoint values, we loaded the chambers on a single device with vancomycin, tetracycline, and kanamycin and assayed the antibiotic susceptibility of the kanamycin resistant strain of *E. coli* MG1655 we created (Fig. 4.5). We used common breakpoints for vancomycin (susceptible ≤ 2 μg mL^{-1}, resistant > 2 μg mL^{-1}), tetracycline (susceptible ≤ 1 μg mL^{-1}, intermediate = 2 μg mL^{-1}, resistant > 2 μg mL^{-1}), and gentamicin (susceptible ≤ 2 μg mL^{-1}, intermediate = 4 μg mL^{-1}, resistant > 4 μg mL^{-1}). As there are no published breakpoints available for kanamycin, we instead used the values for the structurally related aminoglycoside, gentamicin against aerobic bacteria. The ten chambers of the device were divided into three chambers for each antibiotic vancomycin (2, 4, 8 μg mL^{-1}), tetracycline (0.5, 1, 2 μg mL^{-1}), and kanamycin (1, 2, 4 μg mL^{-1}) and one chamber for a control containing no antibiotic. After loading and incubation (18 h), we observed growth in the control chamber and at all concentrations of kanamycin and vancomycin. The bacterial strain grew at the lowest two concentrations of tetracycline but not at the highest concentration. Therefore the phenotype of this organism was determined to be vancomycin

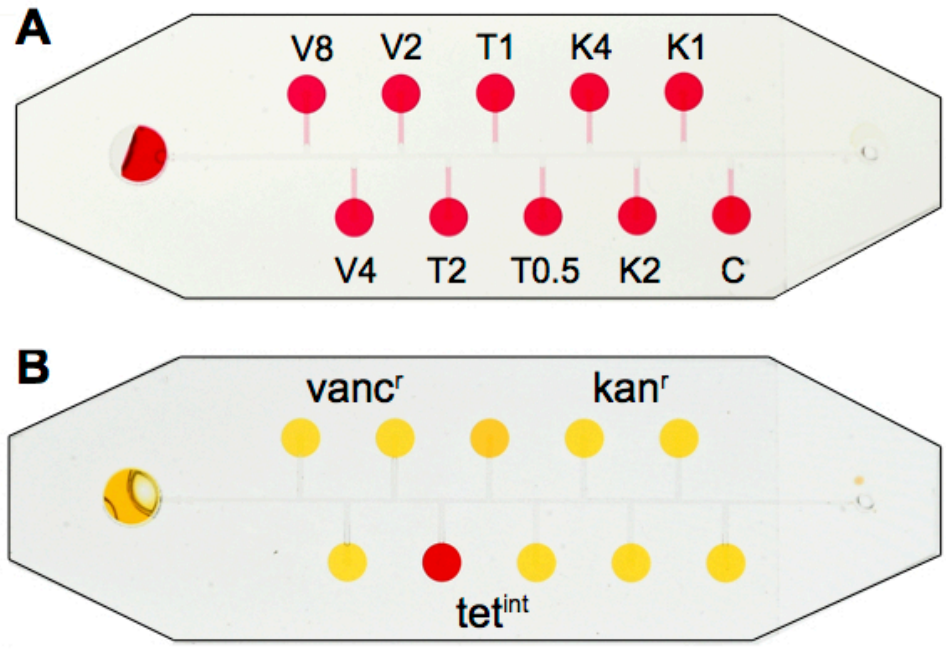

Figure 4.5: Multiplexed antibiotic resistance screening. A series of images depicting the testing of three different antibiotics against a kanamycin resistant strain of *E. coli* MG1655 in a single device using published breakpoint values of antibiotic concentration. A) An image of the device loaded with antibiotics before incubation. The concentration of antibiotics (in μg mL^{-1}) vancomycin (V), tetracycline (T), and kanamycin (K) is indicated adjacent to each chamber; C indicates a control chamber that contained no antibiotic. B) An image of the device after 18 h. The MIC is > 8 μg mL^{-1} for vancomycin, 2 μg mL^{-1} for tetracycline, and > 4 μg mL^{-1} for kanamycin. These results indicate that the phenotype for this organism is tetracycline intermediate (tet^{int}), kanamycin resistance (kan^{r}), and vancomycin resistant ($vanc^{r}$). A black line was drawn around the edge of the device to aid in visualization.

resistant (as to be expected for all Gram-negative bacteria), tetracycline intermediate, and kanamycin resistant. Tetracycline inhibits the growth of this strain; vancomycin and kanamycin do not. These assays can be critical in a clinic as they aid in the prescription of effective antibiotics to treat infections. The device described in this study makes it possible to carry out these assays on a pre-loaded diagnostic platform that is simple and portable.

4.5 Conclusion

We demonstrate a portable microfluidic device for determining the MIC of antibiotics against a range of bacteria that reproduces values measured by dilution methods. This device introduces a new capability for loading and isolating liquid samples in dead-end chambers that contain preloaded reagents by designing the system so that the entry of liquid is followed by air or oil (Linder 2005, Chen 2006, Adamson 2006). The influx of air or oil provides a physical barrier that isolates the sample and compartmentalizes it in individual chambers filled with reagents. This characteristic is particularly useful when working with pathogens as the device isolates the user from the chamber contents. The device requires minimal equipment for loading (i.e. a pipette) and the analysis is performed by observing a colorimetric change of a soluble indicator of bacterial growth. The autonomous mechanism of fluid handling in this device coupled with a simple readout may help bridge the gap to clinical use and the operation of diagnostic systems in resource poor settings. The approach is technically simple and offers a route to reduce the cost of chip-based assays and to increase their

accessibility as clinical diagnostics. We envision that this platform will have applications that extend beyond measuring MICs in which a sample is tested in many different conditions or assays in parallel.

The application of the device described in this study for MIC determination is particularly germane to current trends in combating microbial resistance and antibiotic longevity (Benveniste 1973, Wash 2000, Mouton 2011). It has the potential to improve the effectiveness of selecting antibiotics and doses against specific microbial strains that cause infections and may provide an opportunity for tracking bacterial resistance geographically and over time aiding in the prescription of drugs on a regional basis. As it requires little additional equipment for use, this platform is useful for areas that lack extensive lab infrastructure.

The same gas permeability of PDMS that enables degas driven flow also presents challenges. For example, additional measures are required to assay strict anaerobes. Furthermore, the permeability of PDMS to water vapor requires the incubation of devices in a humid environment. It is possible that hydrophobic compounds will be absorbed by PDMS, so care must be taken when extending the device for use with such reagents (Toepke 2006). Fortunately, many antibiotics are hydrophilic and electrostatically charged in solution, which will reduce their absorption by PDMS and any changes in antibiotic concentration. Furthermore, antibiotic solutions are in contact with the PDMS chambers only during their evaporation, resuspension, and incubation (less than 20 h). During

their longest period of contact with PDMS, the devices are under vacuum and the antibiotics are deposited as solids, which may provide a barrier to their absorption by PDMS. Alternatively, the incorporation of other polymers that support the degas driven flow mechanism, or methods for coating the channel walls can be explored for applications where PDMS is not suitable (Sasaki 2010).

This device offers several advantages over other MIC assays. The platform is portable and reduces: reagent use, sample volume, exposure of the user to the microorganism under study, incubator space, and the necessity of extensive laboratory infrastructure. As long as the ambient environment is warm enough to support bacterial growth, the devices can be operated in a range of environments outside of clinical labs. Using a household vacuum sealer and commercial plastic bags, we found the devices can be degassed and stored in vacuum-sealed bags for at least 12 days prior to their use; after 80 days the devices did not load completely. Improvements in packaging methods are expected to eliminate the need to have a vacuum source on site and provide a mechanism for maintaining the sterility of devices. Although the preparation of the device requires multiple pipetting steps to load reagents into the microchambers, configuring the relative position of the chambers on a device to the spacing of 384 or 1536 wells will enable antibiotics to be deposited in parallel using a liquid handling robot. Regardless of how the antibiotics are loaded, the end-user is insulated from the preloading stage, and only performs one pipetting step to load the sample.

Our use of a pH indicator provides a general route for the colorimetric measurement of bacterial growth on-chip. Incorporating a fluorescent indicator of cell growth and taking advantage of the sensitivity of instruments for measuring fluorescence may provide a mechanism for decreasing the time for detection. By increasing the number of chambers on a device, the difference in the concentration of antibiotic (or reagent) in the chambers could be reduced to increase the resolution of MIC measurements. Increasing the number of chambers would also provide opportunities for analyzing multiple antibiotics, combinations of antibiotics, and multiple samples in parallel. Finally, our microfluidic platform is not limited to assaying the toxicity of antibiotics—we envision it will have applications in other assays in which the reagents are dispensed, dried, and stored in devices under vacuum until their use.

4.6 Acknowledgments

We thank Tim Paustian for helpful discussions. This research was supported by a Searle Scholar Award, the Alfred P. Sloan Research Foundation, and the Keck Foundation.

Chapter 4 contains material originally published as: Cira NJ, Ho JY, Dueck ME, Weibel DB (2012) A self-loading microfluidic device for determining the minimum inhibitory concentration of antibiotics. Lab on a Chip 12(6): 1052-1059.

4. 7 References

Adamson DN, Mustafi D, Zhang JX, Zheng B, Ismagilov RF (2006) Production of arrays of chemically distinct nanolitre plugs via repeated splitting in microfluidic devices. Lab Chip 6(9):1178-86.

Benveniste R, Davies J (1973) Mechanisms of antibiotic resistance in bacteria. Annu Rev Biochem. 42:471-506.

Boedicker JQ, Li L, Kline TR, Ismagilov RF (2008) Detecting bacteria and determining their susceptibility to antibiotics by stochastic confinement in nanoliter droplets using plug-based microfluidics. Lab Chip 8(8):1265-72.

Chen DL, Ismagilov RF (2006) Microfluidic cartridges preloaded with nanoliter plugs of reagents: an alternative to 96-well plates for screening. Curr Opin Chem Biol. 10(3): 226–231.

Chen CH, Lu Y, Sin ML, Mach KE, Zhang DD, Gau V, Liao JC, Wong PK (2010) Antimicrobial susceptibility testing using high surface-to-volume ratio microchannels. Anal Chem 82(3):1012-9.

Chin CD, Linder V, Sia SK (2007) Lab-on-a-chip devices for global health: past studies and future opportunities. Lab Chip 7(1):41-57.

Dimov IK, Basabe-Desmonts L, Garcia-Cordero JL, Ross BM, Park Y, Ricco AJ, Lee LP (2011) Stand-alone self-powered integrated microfluidic blood analysis system (SIMBAS). Lab Chip 11(5):845-50.

Duffy DC, McDonald JC, Schueller OJ, Whitesides GM (1998) Rapid Prototyping of Microfluidic Systems in Poly(dimethylsiloxane). Anal Chem. 70(23):4974-84.

Eun YJ, Utada AS, Copeland MF, Takeuchi S, Weibel DB (2011) Encapsulating bacteria in agarose microparticles using microfluidics for high-throughput cell analysis and isolation. ACS Chem Biol. 6(3):260-6.

Ge B, Bodeis S, Walker RD, White DG, Zhao S, McDermott PF, Meng J (2002) Comparison of the E-test and agar dilution for in vitro antimicrobial susceptibility testing of *Campylobacter*. J Antimicrob Chemother. 50(4):487-94.

Hosokawa K, Sato K, Ichikawa N, Maeda M (2004) Power-free poly(dimethylsiloxane) microfluidic devices for gold nanoparticle-based DNA analysis. Lab Chip 4(3):181-5.

Kim KP, Kim YG, Choi CH, Kim HE, Lee SH, Chang WS, Lee CS (2010) *In situ* monitoring of antibiotic susceptibility of bacterial biofilms in a microfluidic device. Lab Chip 10(23):3296-9.

Levy SB, Marshall B (2004) Antibacterial resistance worldwide: causes, challenges and responses. Nat Med. 10(12 Suppl):S122-9.

Linder V, Sia SK, Whitesides GM (2005) Reagent-loaded cartridges for valveless and automated fluid delivery in microfluidic devices. Anal Chem. 77(1):64-71.

Mouton JW, Ambrose PG, Canton R, Drusano GL, Harbarth S, MacGowan A, Theuretzbacher U, Turnidge J (2011) Conserving antibiotics for the future: new ways to use old and new drugs from a pharmacokinetic and pharmacodynamic perspective. Drug Resist Updat. 14(2):107-17.

Neu HC (1992) The crisis in antibiotic resistance. Science 257(5073):1064-73.

Peitz I, van Leeuwen R (2010) Single-cell bacteria growth monitoring by automated DEP-facilitated image analysis. Lab Chip 10(21):2944-51.

Duffy DC, McDonald JC, Schueller OJA, Whitesides GM (1998) Rapid Prototyping of Microfluidic Systems in Poly(dimethylsiloxane). Anal. Chem. 70(23): 4974–4984.

Toepke MW, Beebe DJ (2006) PDMS absorption of small molecules and consequences in microfluidic applications. Lab Chip 6(12):1484-6.

Walsh C (2000) Molecular mechanisms that confer antibacterial drug resistance. Nature 406(6797):775-81.

Williams JD (1990) Prospects for standardization of methods and guidelines for disc susceptibility testing. Eur J Clin Microbiol Infect Dis. 9(7):496-501.

Xia Y, Whitesides GM (1998) Soft Lithography. Annual Review of Materials Science 28: 153-184.

Yager P, Edwards T, Fu E, Helton K, Nelson K, Tam MR, Weigl BH (2006) Microfluidic diagnostic technologies for global public health. Nature 442(7101):412-8.